Spin Effects on Decay Dynamics of Charge-Separated States Generated by Photoinduced Electron Transfer in Zinc Porphyrin−Naphthalenediimide Dyads

Yukie Mori,*,† Yoshio Sakaguchi, and Hisaharu Hayashi

Molecular Photochemistry Laboratory, RIKEN, The Institute of Physical and Chemical Research, Hirosawa, Wako, Saitama, 351-0198, Japan

Received: September 10, 2001; In Final Form: February 25, 2002

Photoexcitation of zinc porphyrin−bridge−naphthalenediimide (ZP−B−NI) dyads, **1** and **2**, generated the short- and long-distance charge-separated (CS) states, [ZP$^{\bullet+}$−B−NI$^{\bullet-}$], through the intramolecular electron-transfer from excited ZP to NI in solvents of various polarity. The energy level of [ZP$^{\bullet+}$−B−NI$^{\bullet-}$] was either higher (in benzene and 1,4-dioxane) or lower (in solvents of higher polarity) than that of ^{3}ZP*−B−NI. When generated in the singlet spin state, the short-distance CS state derived from **1** rapidly (10^9-10^{10} s^{-1}) decayed through the charge recombination (CR) leading to the ground state. On the other hand, when generated from the triplet excited state of **1**, the decay of the CS state was much slower and showed magnetic field effects attributable to the level-crossing mechanism. For the long-distance CS state derived from **2**, the decay dynamics and its magnetic field dependence exhibited quite different features. To examine the effects of a neighboring additional radical on the decay dynamics of these CS states, three-spin CS states [ZP$^{\bullet+}$−B−NI$^{\bullet-}$−R•] were generated from **1R•** and **2R•**, in which 2,2,6,6-tetramethyl-1-piperidinoxy radical (R•) was connected to the NI part in **1** and **2**, respectively. The decay rate of [ZP$^{\bullet+}$−B−NI$^{\bullet-}$−R•] derived from **1R** • was much faster than that of [ZP$^{\bullet+}$−B−NI$^{\bullet-}$] derived from **1**. For the CS state generated from **2R•**, the initial decay could be retarded compared to the CS state from **2** through the equilibration between the doublet and quartet spin states. The observed effects of R• on the decay processes of the CS states are attributed to the alteration of the energy gap between the states with different spin multiplicities and to the efficient conversion between the doublet and quartet spin states induced by the dipole−dipole interaction between NI$^{\bullet-}$ and R•.

1. Introduction

Photoinduced charge separation processes of donor−bridge−acceptor (D−B−A) systems have been extensively investigated as mimicry of the initial event occurring in the photosynthetic reaction center. Enormous efforts have been made toward efficient formation of long-lived charge-separated (CS) states. The most commonly used strategy is multistep electron-transfer (ET) in arrays of donors and acceptors, in which the opposite charges are separated farther and farther through the sequential electron (or hole) migration processes.[1−4] Effects of molecular conformation and bridge structures on intramolecular ET rates have also attracted attentions.[5,6] In most cases studied so far, the initial charge separation takes place from the singlet excited state of D (or A) to give the intramolecular radical ion-pair, [D$^{\bullet+}$−B−A$^{\bullet-}$], in the singlet ($|S\rangle$) spin state. Within the lifetime of this intermediate or during the subsequent processes such as charge shift reactions, the spin state of the pair is evolved to generate population of the triplet ($|T\rangle$) state through the $|S\rangle \leftrightarrow |T\rangle$ conversion induced by various magnetic interactions.[7,8] In multistep ET processes, variation in separation distance between D$^{\bullet+}$ and A$^{\bullet-}$ alters not only the rates of the charge recombination (CR) processes but also the magnitude of the exchange interaction (J). The J value is one of the important quantities governing the efficiencies of the spin conversion processes,[7−10] although its magnitude is usually much smaller (typically $|J| \leq 10^{-2}$ kJ mol^{-1}) than the thermal energy at an ambient temperature. As long as the CR reactions take place obeying the spin conservation rule, the decay dynamics of the CS states can be largely influenced by the $|S\rangle \leftrightarrow |T\rangle$ conversion rates. Understanding the spin dynamics of the CS states is indispensable to clarify the dynamic aspects of their formation and decay processes. For several CS states, indeed, the decay curves exhibited biphasic nature due to the interconversion of the $|S\rangle$ and $|T\rangle$ states and/or affected by external magnetic fields.[11] So far, however, studies focused on effects of the spin multiplicity in the ET reactions have been quite limited.[10−14] Spin dynamics of radical ion-pair states generated via photoinduced charge separation have also been investigated by means of time-resolved EPR techniques,[15−17] although, in many of these studies, photoexcitation has been carried out in rigid matrixes or liquid crystals not in fluid solution.

Recently, we reported that the presence of an additional radical in the proximity of either D$^{\bullet+}$ or A$^{\bullet-}$ largely accelerates the spin conversion of the CS state, and that the lifetime of the CS state was increased by such enhancement of the spin conversion.[18a] Furthermore, the effects of neighboring unpaired electron(s) were also observed on the product yields or decay rates for ion-pairs[19] and chain-linked biradicals.[20] It is expected that the presence of an additional radical can influence the decay dynamics of various type of CS states, and such spin effects can be utilized as a unique approach toward formation of long-lived CS states.

In the present study, we demonstrate that the spin chemical approach can be applied to increase in the lifetime of CS states formed from the photosynthetic models, and we discuss the relationship between the spin−spin interactions for each pair

* To whom correspondence should be addressed.
† Present address: PRESTO, JST, c/o Prof. H. Imahori, Department of Molecular Engineering, Graduate School of Engineering, Kyoto University, Yoshidahon-machi, Sakyo-ku, Kyoto 606-8501, Japan. E-mail: ymori@mee3.moleng.kyoto-u.ac.jp.

10.1021/jp013453e CCC: $22.00
Published on Web 04/11/2002

TABLE 1: Singlet Excitation Energies (E_S), Fluorescence Quantum Yields Relative to that of Zn(ttp) (Φ_{FL}/Φ^0_{FL}), Efficiencies (Φ^S_{CS} or Φ^D_{CS}) and Rate Constants (k^S_{CR}) of CS, and Free Energy Changes Accompanying CS from ^{1}ZP* (ΔG^S_{CS}), CS from ^{3}ZP* (ΔG^T_{CS}), and CR Leading to the Ground State (ΔG^S_{CR}) for 1, 1R•, 2, and 2R• in Various Solvents at 293 K

			1 (or **1R•**)						**2** (or **2R•**)					
solvent	ϵ[a]	E_S[b]	Φ_{FL}/Φ^0_{FL}[c]	Φ^S_{CS}[c,d]	k^S_{CS}[e]	ΔG^S_{CS}[f]	ΔG^T_{CS}[f]	ΔG^S_{CR}[f]	Φ_{FL}/Φ^0_{FL}[c]	Φ^S_{CS}[c,d]	k^S_{CS}[e]	ΔG^S_{CS}[f,g]	ΔG^T_{CS}[f,g]	ΔG^S_{CR}[f,g]
benzene	2.282	200	0.075	0.93	6.2	< 0	> 0	NA[h]	0.089	0.91	5.1	< 0	> 0	NA[h]
			0.058	0.7					0.065	0.7				
dioxane	2.219	199	0.095	0.91	5.4	< 0	> 0	NA[h]	0.14	0.86	3.5	< 0	> 0	NA[h]
			0.066	0.7					0.11	0.7				
PenOAc	4.79	199	0.076	0.92	6.9	≤ −49	≤ 0	≥ −150	0.089	0.91	5.8	< −49	< 0	> −150
			0.066	0.8					0.086	0.9				
THF	7.52	199	0.069	0.93	7.7	−55	−6	−144	0.085	0.92	6.1	−62	−13	−137
			0.079	0.9					0.075	0.9		(−36)	(+13)	
PrCN	24.83	199	0.084	0.92	6.2	−76	−27	−123	0.084	0.92	6.2	−85	−36	−114
			0.074	0.8					0.084	0.9		(−57)	(−8)	
MeCN	36.64	198	0.12	0.88	4.1	−78	−30	−120	NA[i]	NA[i]	4.6[j]	−87	−39	−111
			0.11	0.8					0.11	≤ 0.9		(−59)	(−11)	

[a] Relative dielectric constant of the solvent at 293 K. ref 74. [b] Unit: kJ mol^{-1}. Calculated from eq 1 with the use of τ_0 value of 2.0 ns for benzene or 1.75 ns for the other solvents. [c] Upper: for **1** or **2**; lower for **1R•** or **2R•**. [d] Estimated from eq 2a or 2b. [e] Unit: 10^9 s^{-1}. [f] Unit: kJ mol^{-1}. [g] The values in the parentheses are the free energy changes for ET from ZP* to B_2. [h] Not available. Only the possible range was determined to be $-200 < \Delta G^S_{CR} < -150$ kJ mol^{-1}. [i] Not available because of low solubility. [j] Based on the Φ_{FL}/Φ^0_{FL} values of **2R•**.

CHART 1

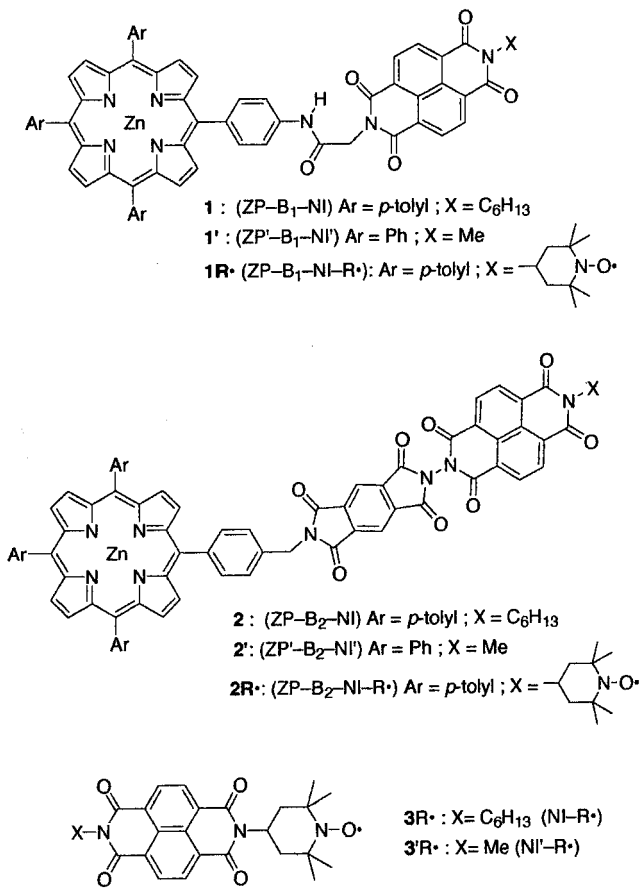

of radicals and the characteristic features of the spin effects on the decay dynamics of the CS states. D−B−A compounds **1** and **2** (Chart 1) were used to generate the short- and long-distance two-spin CS states, respectively. As the precursors of the three-spin CS states, **1R•** and **2R•** were used, in which 2,2,6,6-tetramethyl-1-piperidinoxy (TEMPO) radical was connected to the NI part. We have investigated the decay dynamics and their magnetic field dependence for the CS states derived from these precursors by means of a nano-second laser flash photolysis technique. The major findings are as follows: (i) Large differences in the decay processes were observed between the short- and long-distance CS states not only due to the change in CR rate but also through the alteration of the spin dynamics. (ii) Despite such differences, the presence of the additional radical (R•) affected the decay dynamics of the CS states by the same mechanism for both **1R•** and **2R•**. (iii) By addition of R•, retardation of the initial decay can be achieved for the CS state derived from the singlet excited state of **2** through enhancement of the spin conversion efficiency.

2. Results

2.1. Photoinduced Charge Separation. Photophysical properties of **1**, **1R•**, **2**, and **2R•** were examined by steady-state UV−vis and fluorescence spectroscopy in solvents of various polarity such as benzene, THF, and MeCN. The visible absorption spectra of these dyads showed the Q-bands characteristic for zinc porphyrins at 595 and 555 nm ($\epsilon_{max} \approx 2 \times 10^4$ M^{-1} cm^{-1}). No significant difference from the absorption spectrum of zinc 5,10,15,20-tetrakis(4-methyl-phenyl)-21*H*,23*H*-porphinate [Zn(ttp)] was observed for **1**, **1R•**, **2**, and **2R•**. Although TEMPO radical exhibits a broad absorption band at 400−530 nm, its intensity is much lower than that of the Q-band of Zn(ttp). Thus, irradiation of **1**, **1R•**, **2**, and **2R•** with long wavelength light (λ > 500 nm) selectively excites the ZP part to generate its lowest excited singlet state (^{1}ZP*).

The fluorescence spectra of **1**, **1R•**, **2**, and **2R•** showed the same shape and maximum wavelengths (∼600 and 650 nm) as those of Zn(ttp), and no other emission band was observed. Each of their singlet excitation energies (E_S) was determined to be 198−200 kJ mol^{-1} from the 0,0 band of each fluorescence spectrum. Table 1 summarizes the E_S values and the fluorescence quantum yields relative to that of Zn(ttp), Φ_{FL}/Φ^0_{FL}. The fluorescence from ^{1}ZP* was strongly quenched in these dyads, suggesting that intramolecular ET from ^{1}ZP* to NI took place to give the charge-separated (CS) state, [ZP$^{\bullet+}$−B−NI$^{\bullet-}$(−R•)]. Such intramolecular ET reactions have been reported for a number of zinc porphyrin−diimide systems.[6,21,22]

Formation of the CS state was unequivocally revealed by transient absorption spectroscopy. Figure 1 shows the absorbance change observed upon excitation of **2** with a 532 nm laser pulse in benzene. The spectrum recorded at 12−32 ns after excitation (solid line) exhibited positive peaks at 470 and 605 nm and a negative one at 550 nm. The positive peaks were assigned to the absorption bands of NI$^{\bullet-}$ in the CS state, on the basis of comparison with the absorption spectrum of the radical

SCHEME 1: Photochemical Reaction Pathways of (a) 1 and 2 in Nonpolar Solvents, (b) 1 and 2 in Polar Solvents, (c) 1R• and 2R• in Nonpolar Solvents, and (d) 1R• and 2R• in Polar Solvents[a]

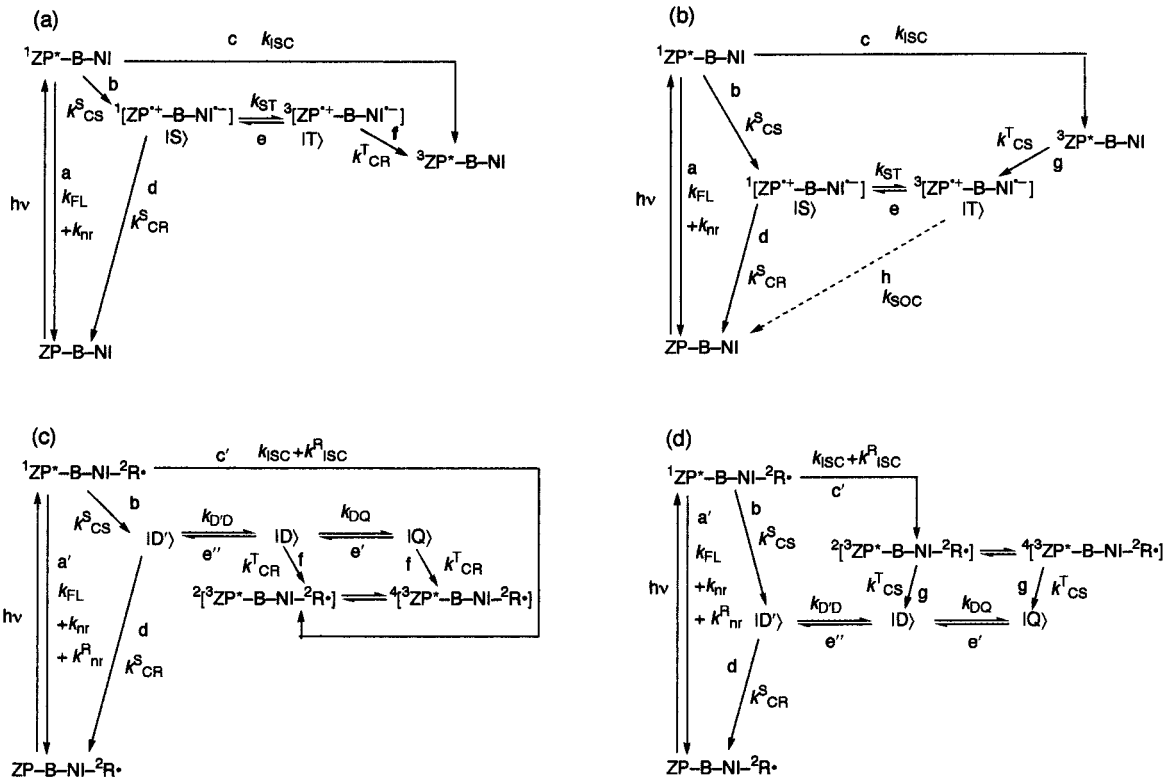

[a] Intermediate [ZP•+−B2•−−NI(−R•)] is omitted for clarity. in (c) and (d), |D′⟩ and |D⟩ stand for the doublet CS state, 2[ZP•+−B−NI•−−R•], whereas |Q⟩ for the quartet one, 4[ZP•+−B−NI•−R•]. The arrows and *k*'s represent the following processes and their rates: **a** and **a′**: fluorescence (k_{FL}), nonradiative deactivation (k_{nr}), and radical-induced decay (k^R_{nr}) of ^{1}ZP*; **b**: ET from ^{1}ZP* to NI; **c** and **c′**: intersystem crossing (ISC) from ^{1}ZP* to ^{3}ZP* (k_{ISC}) and enhanced ISC by R• (k^R_{ISC}); **d**: charge recombination (CR) to give the ground state; **e**: |S⟩ ↔ |T⟩ conversion; **e′** and **e″**: |D⟩ ↔ |Q⟩ and |D′⟩ ↔ |D⟩ conversions; **f**: CR to give ^{3}ZP*; **g**: ET from ^{3}ZP* to NI; **h**: SOC-induced CR to give the ground state.

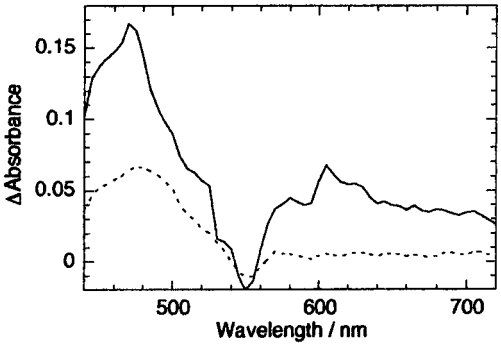

Figure 1. Transient absorption spectra measured upon excitation of **2** with a 532 nm laser pulse in deaerated benzene at 293 K. The solid and dotted lines denote the spectra acquired in time windows of 12−32 and 200−800 ns after excitation, respectively.

anion of *N*,*N*′-dihexylnaphthalene-1,8:4,5-tetracarboxydiimide ($C_6NI^{\bullet-}$) measured in MeCN [λ_{max} = 473 ($\epsilon = 3.4 \times 10^4$ M^{-1} cm^{-1}), 515 (sh), 590 (sh), and 607 nm ($\epsilon = 8.9 \times 10^3$)]. The negative peak is due to the depletion of the ground state of ZP. The absorption spectrum of radical cation of zinc 5,10,15,20-tetraphenyl-21*H*,23*H*-porphinate [Zn(tpp)$^{\bullet+}$] measured in CH_2Cl_2[23] or MeCN shows very broad absorption in 500−750 nm and an intense absorption band at 406 nm. Although no absorption band assignable to ZP$^{\bullet+}$ was distinguished in the transient spectrum shown in Figure 1, its absorption should have some contribution to the positive absorbance change in 600−750 and 440−480 nm. As shown by the dotted line in Figure 1, the spectrum recorded at t > 200 ns exhibited a broad absorption band at 470 nm, which did not substantially decay within the monitored time window (t < 950 ns). This long-lived component was assigned to the T−T absorption of ^{3}ZP*.[24] For the other dyads, the transient absorption bands assignable to the CS states were also observed. Thus, it has been clearly demonstrated that irradiation of dyads **1**, **1R•**, **2**, and **2R•** generated the CS states through intramolecular ET from ^{1}ZP* to NI. The photochemical reaction pathways are shown in Scheme 1. Here, |D′⟩, |D⟩, and |Q⟩ are [ZP•+−B−NI•−−R•] with different spin states, as shown in Appendix.

In the cases of **1** and **2**, we can assume that the fluorescence quenching takes place exclusively through charge separation (CS) (process **b** in Scheme 1a,b), because the energy transfer from ^{1}ZP* to NI is thermodynamically unfavorable, and because neither **1** nor **2** contains any heavy atom which could enhance the intersystem crossing (ISC) to the ^{3}ZP* state (process **c**). The rate constant of CS (k^S_{CS}) can be estimated by

$$k^S_{CS} = \tau_0^{-1} (\Phi^0_{FL}/\Phi_{FL} - 1) \quad (1)$$

where τ_0^{-1} (= $k_{FL} + k_{nr} + k_{ISC}$) is the decay rate of ^{1}ZP* through the processes other than CS (fluorescence emission, nonradiative decay, and ISC). The reported fluorescence lifetime of Zn(ttp) (2.0 ns in toluene; 1.75 ns in dimethyl sulfoxide (DMSO))[24b] was used as τ_0. As shown in Table 1, the k^S_{CS} values were in a range of (4−8) × 10^9 s^{-1} and almost independent of the solvent polarity. Such insensitivity of the photoinduced CS rate to the solvent polarity has been reported for several D−B−A compounds.[18a,25]

The quantum yield of CS in the singlet manifold (Φ^{S}_{CS}) for **1** and **2** is equal to the efficiency of the fluorescence quenching (Φ_q), as represented by eq 2a

$$\Phi^{S}_{CS} = \Phi_q = 1 - [\Phi_{FL}/\Phi^{0}_{FL}] \quad (2a)$$

The k^{S}_{CS} values for **1R•** and **2R•** can be assumed to be the same as the corresponding values for **1** and **2**, respectively, and the decreases in Φ_{FL}(**1R•** or **2R•**) from Φ_{FL}(**1** or **2**) may be caused by nonradiative processes due to R•.[26] Thus, the quantum yield for formation of the CS state with a total spin multiplicity of doublet (Φ^{D}_{CS}) can be expressed by eq 2b

$$\Phi^{D}_{CS}(\mathbf{1R\bullet} \text{ or } \mathbf{2R\bullet}) = \Phi^{S}_{CS}(\mathbf{1} \text{ or } \mathbf{2}) \times [\Phi_{FL}(\mathbf{1R\bullet} \text{ or } \mathbf{2R\bullet})/\Phi_{FL}(\mathbf{1} \text{ or } \mathbf{2})] \quad (2b)$$

As shown in Table 1, the Φ^{D}_{CS} values of **1R•** and **2R•** in benzene and dioxane were somewhat lower than the Φ^{S}_{CS} values of **1** and **2**, respectively. The energy transfer from ^{1}ZP* to R• by the Förster mechanism might contribute to the fluorescence quenching to some extent in these solvents.[26] The efficiency of this process, however, is probably low because the excitation energy of R• is higher than that of ZP and because the spectral overlap of the absorption of R• with the fluorescence emission from ^{1}ZP* is poor. Alternatively, ^{1}ZP* may be quenched by R• through the enhanced ISC.[26] In polar solvents such as THF and MeCN, the Φ^{D}_{CS} values of **1R•** and **2R•** were almost the same as the Φ^{S}_{CS} values of **1** and **2**, respectively, indicating that contribution of the quenching by R• was negligible. It is noteworthy that the Φ^{D}_{CS} values were estimated to be 0.7 or higher in any solvents investigated.

As will be shown in section 3.1, dyad **1** can adopt at least two conformations with somewhat different distances and orientations between the ZP and NI parts. Coexistence of more than one conformers may result in multiexponential fluorescence decay, as was demonstrated for cyclophane-bridged zinc porphyrin−quinone dyads.[27] In such cases, the k^{S}_{CS} value derived from eq 1 does not correspond to the CS rate of any single conformer. The applicability of eq 1 to **2** should be considered with mechanism of the long-distance ET taken into consideration (see section 3.2). Although time-resolved fluorescence measurement is desirable, the important results obtained for the present dyads are (i) that CS from ^{1}ZP* takes place with high efficiency ($\Phi^{S}_{CS} \approx 0.9$ for **1** and **2**) in any solvents investigated, (ii) that ^{1}ZP* state disappeared in subnanosecond time scale, and (iii) that contribution of the R•-induced quenching has only minor contribution to the fluorescence quenching. The second point means that the singlet (or doublet for **1R•** or **2R•**) CS state would be observed instantaneously on excitation with a nanosecond laser pulse, which is consistent with the results of transient absorption spectroscopy.

2.2. MFEs on Decay Dynamics of the CS States Derived from 1 and 1R•. *(a) In Benzene and Dioxane*. Upon excitation of **1** in benzene with a 532-nm laser pulse, the time course of the absorbance change monitored at 470 nm, $\Delta A_{470}(t)$ curve, consisted of two decaying components. The short-lived component decayed within the duration of the laser pulse (<20 ns), whereas the long-lived one was constant at 30−950 ns after excitation. When the absorbance change was monitored at 605 nm, the $\Delta A_{605}(t)$ curve also contained two components, but the intensity of the long-lived component was much lower than that observed at 470 nm. As shown in Figure 1, ^{3}ZP* as well as the CS state absorb 470-nm light, whereas the absorption of ^{3}ZP* is quite small at 605 nm. From these facts, the short-lived species

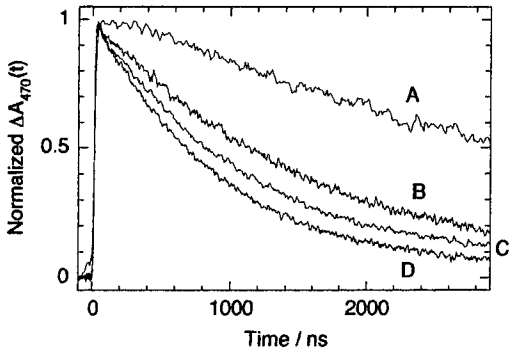

Figure 2. Normalized $\Delta A_{470}(t)$ curves for **1** in various solvents under a zero field. A: PenOAc; B: THF; C: PrCN; D: MeCN.

was assigned to the CS state generated in the $|S\rangle$ state, ^{1}[ZP$^{\bullet+}$−B$_1$−NI$^{\bullet-}$], which rapidly decayed through the spin-allowed CR process to give the ground state (process **d** in Scheme 1a). The long-lived species was assigned to ^{3}ZP*−B$_1$−NI generated through ISC. In dioxane, only the long-lived component was observed, suggesting that the lifetime of ^{1}[ZP$^{\bullet+}$−B$_1$−NI$^{\bullet-}$] was too short to be detected with our apparatus.

The $\Delta A_{470}(t)$ curves measured upon excitation of **1R•** in benzene and dioxane were quite similar to those of **1** except that the intensities were reduced by ∼15% of those of **1**. This decrease in the yields of the CS state and ^{3}ZP* is likely due to other quenching processes, as was suggested by the results of the fluorescence quenching.[28] Application of a magnetic field below 1.7 T did not bring about any detectable change in the $\Delta A_{470}(t)$ curve of **1** or **1R•** in either benzene or dioxane. Thus, the decay of the CS state in these solvents was governed by the spin-allowed CR process which was much faster than the spin evolution.

(b) In Solvents of Medium or High Polarity. In solvents of higher polarity, the decay dynamics of the $\Delta A_{470}(t)$ curve for **1** was quite different from that observed in benzene or dioxane. Figure 2 shows the normalized $\Delta A_{470}(t)$ curves measured upon excitation of **1** in pentyl acetate (PenOAc), THF, butyronitrile (PrCN), and MeCN. Each of the $\Delta A_{470}(t)$ curves decayed in microsecond time region, and the decay rate increased with increasing solvent polarity. In MeCN, the two-step reaction process, ^{3}ZP*−B$_1$−NI → [ZP$^{\bullet+}$−B$_1$−NI$^{\bullet-}$] → ZP−B$_1$−NI, occurred with rate constants of k_1 (= k^{T}_{CS}) = 1.4×10^7 s^{-1} and $k_2 = 1.0 \times 10^6$ s^{-1} for the first and second steps, respectively (Figure 1S). Although ET from ^{1}ZP* took place, the CS state born in the $|S\rangle$ state decayed too fast to be detected, as was the case in dioxane. As a result, only the CS state generated via ET from ^{3}ZP* (process **g** in Scheme 1b) was observed in the transient absorption spectra. The CS state born in the $|T\rangle$ state mainly decayed through the spin conversion to the $|S\rangle$ state (process **e**) followed by CR leading to the ground state (process **d**).

To clarify the spin dynamics of the CS state, we examined MFEs on the $\Delta A_{470}(t)$ curves. Figure 3a shows the $\Delta A_{470}(t)$ curves for **1** under various magnetic fields (B's) in THF. With increasing B, the decay of the $\Delta A_{470}(t)$ curve became faster from 0 to 0.9 T and slower from 0.9 to 1.7 T. To represent the B dependence of the decay behavior of the CS state,[29] we use the $R(B)$ value defined by $R(B) = I_{470}(t_1-t_2, B)/I_{470}(t_1-t_2, 0\text{ T})$, where $I_{470}(t_1-t_2, B)$ and $I_{470}(t_1-t_2, 0\text{ T})$ are the integration values of the $\Delta A_{470}(t)$ curves in the time range of $t_1 \le t \le t_2$ in the presence and absence of B, respectively. An appropriate time range[30] was chosen for each solvent. Figure 4a shows the $R(B)$ vs B plots obtained for **1** in various solvents. The $R(B)$ value exhibited a minimum at 0.9 T in PenOAc and THF. This type

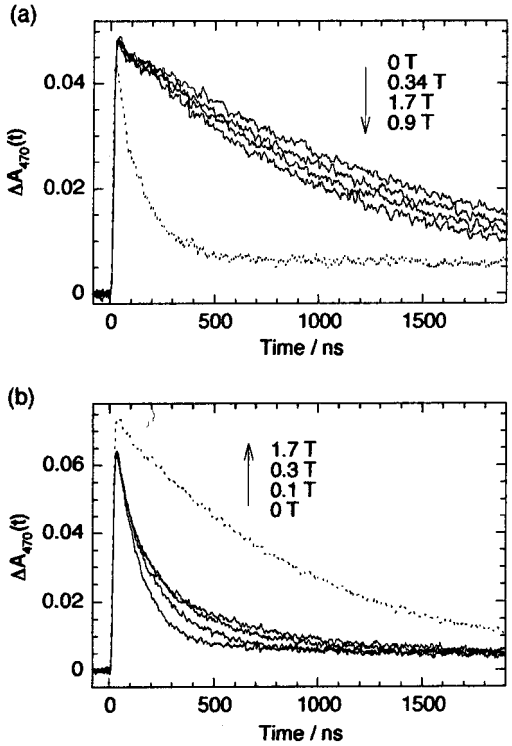

Figure 3. (a) $\Delta A_{470}(t)$ curves for **1** in THF under various B's. The dotted line shows the $\Delta A_{470}(t)$ curve for **1R•** under the same conditions. (b) $\Delta A_{470}(t)$ curves for **1R•** in MeCN under various B's. The dotted line shows the $\Delta A_{470}(t)$ curve for **1** under the same conditions. The B values are indicated in the figures.

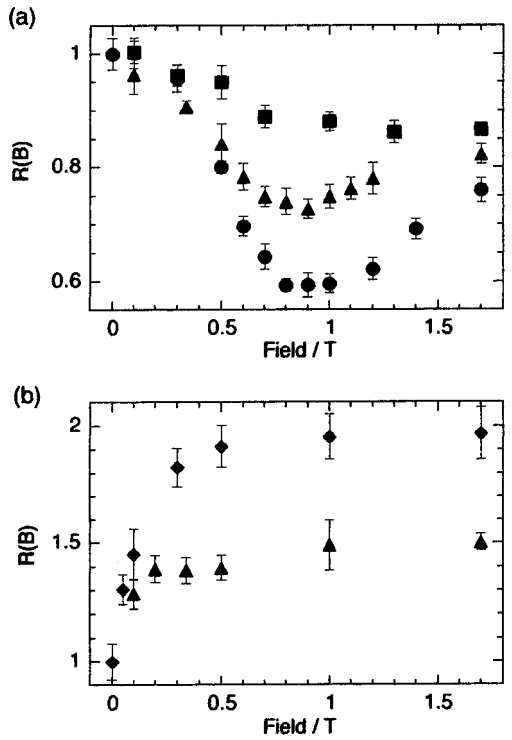

Figure 4. Field dependence of the $R(B)$ values for (a) **1** and (b) **1R•** in various solvents. The symbols represent the following solvents and the time windows for integration: (a) circle: PenOAc (200−800 ns); triangle: THF (500−2500 ns); square: PrCN (100−3100 ns). (b) triangle: THF (100−1000 ns); diamond: MeCN (300−500 ns).

of MFE can be explained by the level-crossing mechanism (LCM),[7,8] as shown in Scheme 2a. The exchange interaction (J) is assumed to be positive in these solvents (see Section 3.3).

SCHEME 2: Energy Levels and Interconversion Processes of the Spin Sublevels of the CS States Derived from (a) 1, (b) 2, and (c) 1R• and 2R•[a]

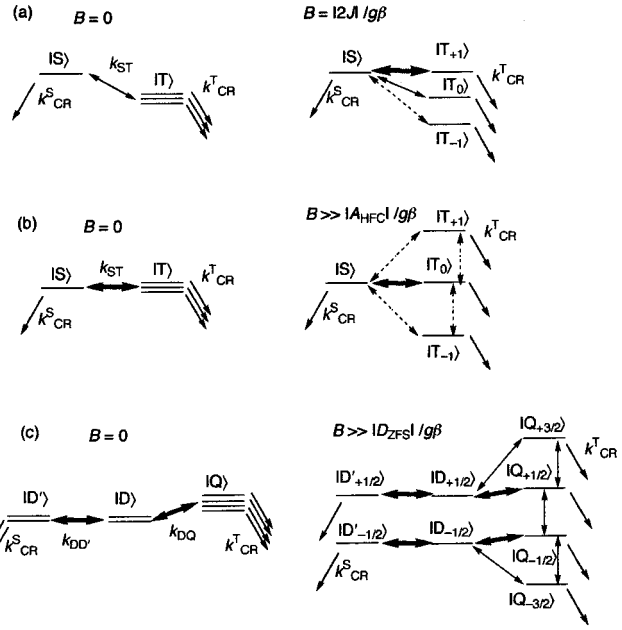

[a] The broken and thick arrows represent less and more efficient conversion processes, respectively, than those represented by the thin solid arrows. in (a), the J Is assumed to be positive.

Under a zero field the HFC-induced $|S\rangle \leftrightarrow |T\rangle$ conversion is inhibited, because the energy levels of the $|S\rangle$ and $|T\rangle$ states are separated by $2|J|$. Under a magnetic field of $B = 2|J|/g\beta$, the energy level of the $|T_{+1}\rangle$ sublevel coincides with that of the $|S\rangle$ state, and therefore the $|S\rangle \leftrightarrow |T_{+1}\rangle$ conversion takes place through the HFC interactions with an effective rate of $10^7 - 10^8$ s^{-1}.

In PrCN, the $R(B)$ value decreased with increasing B from 0 to 1.4 T, where the MFE was almost saturated. The magnitude of the MFE observed in PrCN was much smaller than that observed in PenOAc or THF. In MeCN, the decay of the $\Delta A_{470}(t)$ curve became marginally slower with increasing B from 0 to 1.7 T. The absence of minimum in the $R(B)$ value suggests that the $2|J|/g\beta$ value could be larger than 1.7 T.

The dotted line in Figure 3a shows the $\Delta A_{470}(t)$ curve observed for **1R•** in THF under the same conditions as in the case of **1**. The $\Delta A_{470}(t)$ curve for **1R•** decayed much faster than that observed for **1**. The $\Delta A_{470}(t)$ curve for **1R•** under a zero field could be fit to a single-exponential function with a small fraction of residual component (10% of the initial intensity) remained (Figure 2b−eS). This long-lived component may be attributed to the T−T absorption of the ^{3}ZP* in some impurities or the absorption due to the radical ions formed through either a certain secondary reaction or an intermolecular charge shift process. As shown in Table 2, the observed decay rates were almost the same in PenOAc, THF, PrCN, and MeCN and much larger than that of **1** in MeCN (Figures 1S and 2aS). The different decay kinetics of the CS states derived from **1** and **1R•** clearly indicates that the rate-determining step involves the spin conversion process.

Figure 3b shows the $\Delta A_{470}(t)$ curves for **1R•** in MeCN under various B's. For comparison, the $\Delta A_{470}(t)$ curve for **1** measured under the same conditions was represented by the dotted line. The $\Delta A_{470}(t)$ curve for **1R•** decayed much faster than that for **1**, as was observed in THF (Figure 3a). In the presence of magnetic fields, the $\Delta A_{470}(t)$ curves for **1R•** could not be fit to

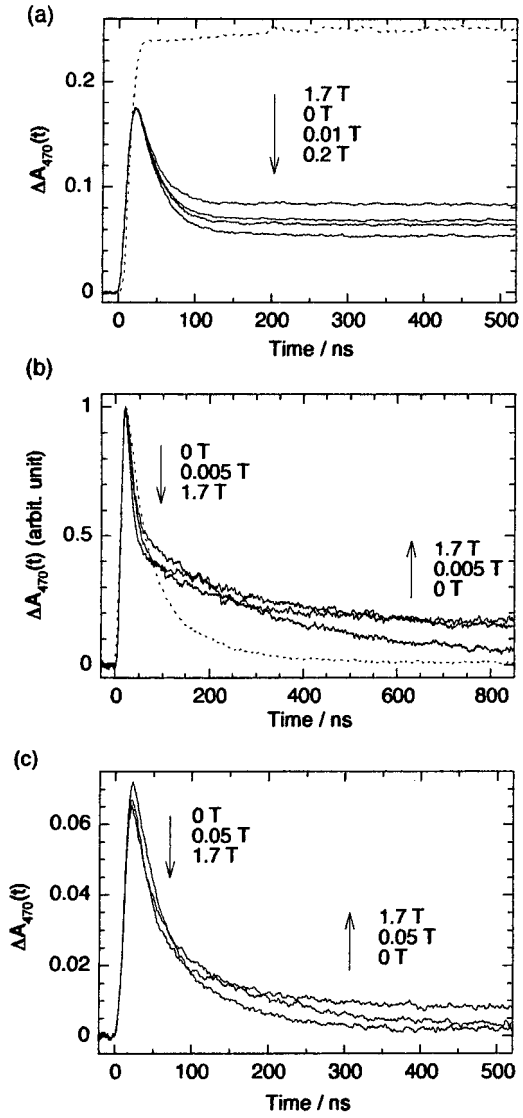

Figure 5. $\Delta A_{470}(t)$ curves for **2** (a) in benzene and (b) in THF under various *B*'s. The dotted lines represent the $\Delta A_{470}(t)$ curves for **2R•** in each solvent under the same conditions. (c) The $\Delta A_{470}(t)$ curves for **2R•** in PrCN under various *B*'s. The *B* values are shown in the figures. In (b), the dotted line is normalized to set the maximal $\Delta A_{470}(t)$ value equal to the corresponding value of the solid line under a zero field.

TABLE 2: Observed Decay Rates and Relevant Rate Constants for the CS States Derived from 1, 1R•, 2, and 2R• under Zero Field

comp.	solvent	observed rates/s^{-1}	k^S_{CR}/s^{-1}	k_{ST}/s^{-1}
1R•	PenOAc	6.1×10^6		
1R•	THF	7.3×10^6		
1R•	PrCN	1.0×10^7		
1R•	MeCN	7.8×10^6		
1	MeCN	1.0×10^6		
2R•	PenOAc	8.6×10^6	3.3×10^7	
2	PenOAc	4.14×10^7, 2.23×10^6	3.2×10^7	2.9×10^6
2	THF	7.02×10^7, 3.56×10^6	5.6×10^7	4.5×10^6

a single-exponential function, and a longer-lived component was observed and its decay became slower with increasing *B* from 0 to 1.7 T. Figure 4b shows that the *R*(*B*) vs *B* plots for **1R•** in MeCN (diamond) and THF (triangle). The *R*(*B*) values increased with increasing *B* from 0 to 1 T and became almost constant at $B \geq 1$ T. In PenOAc, similar MFEs were observed. It is noteworthy that the *B* dependence of the *R*(*B*) value for **1R•** was quite different from that observed for **1**.

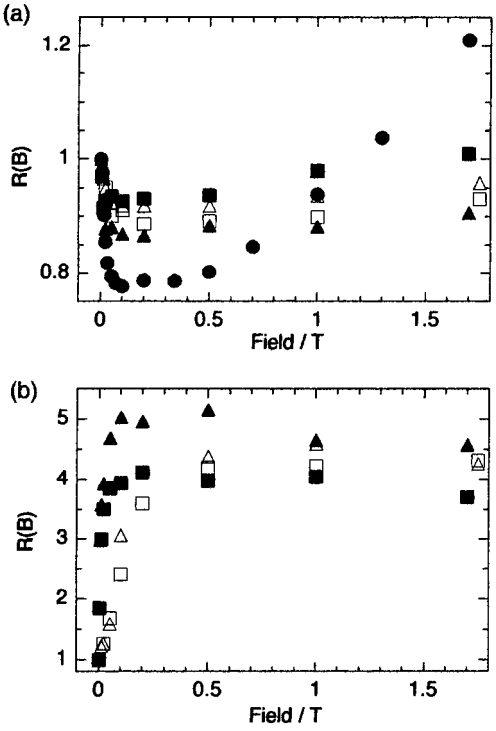

Figure 6. Field dependence of the *R*(*B*) values for **2** and **2R•** in various solvents in (a) early and (b) later time regions. The symbols represent the following solutions and time windows for integration: closed circle: **2** in benzene, (a) 300−800 ns; closed triangle: **2** in THF, (a) 10−210 ns, (b) 800−1800 ns; closed square: **2** in PrCN, (a) 15−55 ns, (b) 400−900 ns; open triangle: **2R•** in THF, (a) 14−30 ns, (b) 400−800 ns; open square: **2R•** in PrCN, (a) 14−34 ns, (b) 400−800 ns.

2.3. MFEs on Decay Dynamics of the CS States Derived from 2 and 2R•. *(a) In Benzene and Dioxane*. Figure 5a shows the $\Delta A_{470}(t)$ curves for **2** in benzene under various *B*'s. Each of the $\Delta A_{470}(t)$ curves consisted of two components. The short-lived component was assigned to the absorption due to the CS state, and the long-lived one was to the T−T absorption of ^{3}ZP*. Because the short-lived component had decayed within about 150 ns, the constant part of the $\Delta A_{470}(t)$ values contained only the contribution from the T−T absorption of ^{3}ZP*−B_2−NI. The yield of ^{3}ZP*−B_2−NI was dependent on *B*, indicating that the ^{3}ZP*−B_2−NI was formed through the intermediary of the CS state (a sequence of processes **b**, **e**, and **f** in Scheme 1a) as well as through ISC (process **c**). The total yield of ^{3}ZP*−B_2−NI is expressed by eq 3

$$\Phi_T(B) = k_{ISC}/(\tau_0^{-1} + k^S_{CS}) + k^S_{CS}/(\tau_0^{-1} + k^S_{CS}) \times \eta_T(B) \quad (3a)$$

$$= (1 - \Phi^S_{CS}) \times \Phi^0_{ISC} + \Phi^S_{CS} \times \eta_T(B) \quad (3b)$$

Here, $\eta_T(B)$ is the fraction of the formation of ^{3}ZP*−B_2−NI from [$ZP^{\bullet+}$−B_2−$NI^{\bullet-}$] born in the $|S\rangle$ state, and Φ^0_{ISC} ($= k_{ISC} \times \tau_0$) stands for the quantum yield of ISC in the absence of CS. The first and second terms in eq 3 represent the contributions from the ISC from ^{1}ZP* to ^{3}ZP* (process **c**) and from the process **f** through the intermediacy of the CS state, respectively. With the use of the observed Φ^S_{CS} value (0.91) and the reported Φ_{ISC} value (0.88)[24b] of Zn(ttp) for Φ^0_{ISC}, the first term amounts only 0.08, which is independent of *B*. Figure 6a (closed circle) shows the *B* dependence of the *R*(*B*) value with the time window of 300−800 ns, which corresponds to the ratio of $\Phi_T(B)/\Phi_T(0$ T). The *R*(*B*) value decreased with increasing *B* from 0 to 0.1

T and increased from 0.1 to 1.7 T, exceeding unity at $B \geq 1.3$ T. The $\Delta A_{470}(t)$ curves measured in dioxane were similar to those observed in benzene except that the decay of the short-lived component was faster than in benzene. The B dependence of $R(B)$ in dioxane was also similar to that observed in benzene.

To examine the effects of R• on the decay of the long-distance CS state, the $\Delta A_{470}(t)$ curve for **2R•** was measured in benzene under the same conditions as the case of **2**. As is shown by the dotted line in Figure 5a, no initial decay was detected, and only the long-lived component assignable to the T−T absorption was observed.[28] The Φ_T (0 T) value of **2R•** in benzene was estimated to be 0.85, which was much higher than that of **2** (0.24). No MFE was observed on the $\Delta A_{470}(t)$ curve for **2R•** below 1.7 T. These results indicated that most part of [$ZP^{\bullet+}-B_2-NI^{\bullet-}-R\bullet$] underwent CR leading to [$^3ZP^*-B_2-NI-R\bullet$] (process **f** in Scheme 1c) under any B between 0 and 1.7 T. In dioxane, the Φ_T (0 T) value of **2R•** was also larger than that of **2** but somewhat smaller than that of Zn(ttp). The Φ_T (B) value of **2R•** slightly decreased with increasing B from 0 to 0.1 T and was constant at $B = 0.1-1.7$ T. No reversion of MFE on the Φ_T (B) value was observed.

(b) In Solvents of Medium or High Polarity. Figure 5b shows the $\Delta A_{470}(t)$ curves for **2** measured in THF under various B's. Each of the $\Delta A_{470}(t)$ curves exhibited biphasic decay. The shape of the transient absorbance spectrum in 440−650 nm was not varied with time from immediately after excitation to 1 μs, indicating that both the short- and long-lived components were assignable to the absorption of the CS state, [$ZP^{\bullet+}-B_2-NI^{\bullet-}$]. The $\Delta A_{470}(t)$ curve for **2** in PenOAc under a zero field was similar to that in THF. In THF, PenOAc, or PrCN, the CS state decayed only through the CR leading to the singlet ground state (Scheme 1b) because formation of $^3ZP^*-B_2-NI$ from ^{3}[$ZP^{\bullet+}-B_2-NI^{\bullet-}$] was thermodynamically unfavorable. From the observed decay rates the k^S_{CR} values in PenOAc and THF were obtained[31] (Table 2). In PrCN, the short-lived component of the $\Delta A_{470}(t)$ curve showed much lower intensity and faster decay than those observed in PenOAc and THF. The results indicated that the k^S_{CR} value increased with increasing solvent polarity (PenOAc < THF < PrCN).

As seen in Figure 5b, the presence of magnetic fields accelerated the decay of the short-lived component and retarded that of the long-lived one. As a qualitative measure of the MFEs on the decay curves, we obtained the $R(B)$ values for each of the components by setting different integration time windows and plotted them against B in Figure 6. The $R(B)$ value of the short-lived component observed in THF (closed triangle) decreased with increasing B from 0 to 0.2 T and then slightly increased with increasing B from 0.2 to 1.7 T, whereas the $R(B)$ value of the long-lived one exhibited MFEs in the opposite direction. Similar biphasic decay and the MFEs in the opposite directions on the decay rates of the short- and long-lived components were previously reported for some long-distance CS states.[11,18a] The MFEs observed in PenOAc and PrCN showed similar trends to that observed in THF. The magnitudes of the MFEs on the decay at early time region increased in the reverse order of k^S_{CR}, that is, PrCN < THF < PenOAc.

The decay dynamics of [$ZP^{\bullet+}-B_2-NI^{\bullet-}$] in these solvents was also affected by the presence of R•. The dotted line in Figure 5b shows the normalized $\Delta A_{470}(t)$ curve measured for **2R•** in THF under a zero field. At early time (t < 70 ns) the decay was slower than that of the $\Delta A_{470}(t)$ curve for **2**, whereas at later time it was much faster than the latter. Figure 5c shows the $A_{470}(t)$ curves for **2R•** in PrCN under different B's. The $\Delta A_{470}(t)$ curve under a zero field was similar to that observed in THF. In these solvents, the $\Delta A_{470}(t)$curves observed for **2R•** under a zero field exhibited only slight deviation from single-exponential decay, whereas each curve contained two components with different decay rates in the presence of magnetic fields. The $R(B)$ vs B plots of the short- and long-lived components observed for **2R•** in THF (open triangle) and PrCN (open square) are shown in Figure 6. Because the deviation of the $A_{470}(t)$ curve from a single-exponential function was rather small, the separation of the short-lived component from the long-lived one may be incomplete. The B dependence of the $R(B)$ values observed in THF and PrCN were quite similar to each other. As is shown in Figure 6a, the magnitude of the MFEs on the $R(B)$ value of the short-lived component for **2R•** was smaller than that observed for **2**. Figure 6b indicates that the $R(B)$ value of the long-lived component increased with increasing B from 0 to 0.5 T and became almost constant under fields of $0.5 \leq B \leq 1.7$ T. Such B dependence of the $R(B)$ value for the long-lived component of **2R•** was qualitatively similar to that observed for **1R•** in THF or MeCN (Figure 3b). It is noteworthy that the B value at which the maximal $R(B)$ value was observed for **2R•** (0.5 T) was higher than that observed for **2** (0.1−0.2 T). The $\Delta A_{470}(t)$ curve measured for **2R•** in PenOAc under zero field decayed more slowly than in THF or PrCN and could be fit to a single-exponential function. The obtained k^S_{CR} value[31] was in good agreement with that derived from the $\Delta A_{470}(t)$ curve for **2** (Table 2). The $R(B)$ values showed MFEs similar to those observed in THF or PrCN, although the magnitude was smaller.

TABLE 3: Selected Geometrical Parameters for the Optimized Structures of 1′ and 2′

parameter[a]	*anti*-**1′**	*syn*-**1′**	**2′**
ψ/°	−79.3	−89.6	−85.7
ϕ_1/°	0.4	0.1	
ϕ_2/°	−2.0	0.0	
ϕ_3 or ϕ_3'/°	112.0	0.1	89.4
ϕ_4 or ϕ_4'/°	86.2	85.2	87.3
θ/°			−90.1
d_{cc}(ZP′, NI′)/Å[b]	13.6	14.9	18.2 (11.7)[d]
d_{ee}(ZP′, NI′)/Å[c]	8.5	9.1	12.6 (6.5)[d]

[a] The definitions are shown in Figure 7. [b] The distance between the Zn atom and the center of the naphthalene ring in NI′. [c] The distance between the C-5 in ZP′ and the closer N atom in NI′. [d] The value in the parenthesis is the corresponding distance between ZP′ and B_2.

3. Discussion

3.1. Molecular Structures of the Dyads. The decay dynamics of the short-distance CS state formed from **1** was quite different from that of the long-distance one from **2**. Variation in the separation distance between $ZP^{\bullet+}$ and $NI^{\bullet-}$ gives rise to changes in the CR rates (k^S_{CR} and k^T_{CR}) and in the magnitudes of the electron spin−spin interactions. To estimate the separation distances in **1**(**R•**) and **2**(**R•**), we carried out ab initio structure optimization of model compounds **1′** and **2′** (see Chart 1) at the HF/3-21G level.

In the optimized structures of **1′** and **2′**, the porphyrin macrocycle is planar, and the peripheral phenyl groups are almost perpendicular to this plane. These structural features are consistent with the results of the X-ray structure analysis of Zn(tpp).[32] Table 3 summarizes the selected torsion angles and the center-to-center and edge-to-edge distances (d_{cc} and d_{ee}, respectively) between ZP′ and the acceptor moieties (NI′ or B_2) in **1′** and **2′**. Two stable conformers of **1′** were obtained as local minima. In one conformer (anti-**1′**), the NI′ group is in anticlinal with respect to the carbonyl oxygen in the bridging amide, and an intramolecular hydrogen-bond is formed between the

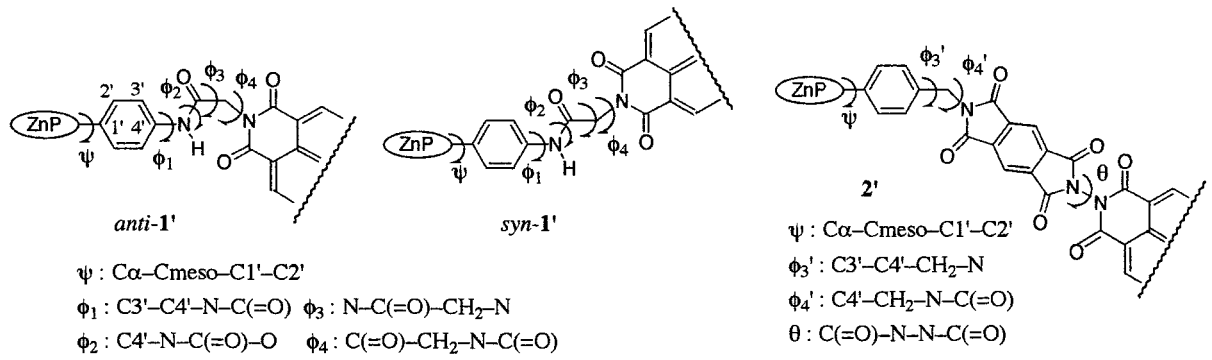

Figure 7. Definition of the torsion angles in **1′** and **2′**.

NH in the bridging amide and the carbonyl oxygen in NI′, as shown in Figure 7. In the other conformer (syn-**1′**), the NI′ group adopts a syn-periplanar orientation with respect to the carbonyl oxygen in the bridging amide. Anti-**1′** is predicted to be more stable by only 0.74 kJ mol^{-1} than syn-**1′**. In polar solvents, a H-bond can be formed between the NH and the solvent molecule, and therefore, the relative stability of the two conformers may be different from that predicted for an isolated molecule in the gas phase. In the optimized structure of **2′**, the diimide parts, B_2 and NI′, are perpendicular to each other. This molecule has rotational freedom around the CH_2-phenylene (at the 5-position of ZP′) and the CH_2-N bonds (ϕ_3' and ϕ_4' in Figure 7). Because of the local pseudo-C_{2v} symmetry of the B_2-NI′ part, however, the rotation around these bonds does not alter the donor−acceptor distances. The separation distance between ZP′ and NI′ in **2′** is by ca. 4 Å larger than that in **1′** (Table 3).

In general, the equilibrium structure of the CS state is different from that of the neutral ground state.[33] Shephard and Paddon−Row suggested that Coulombic interaction can give rise to large structural changes accompanying CS processes in donor−bridge−acceptor compounds even if their structures were thought to be rather rigid.[34] Although their prediction was based on the ab initio calculations for isolated molecules in the gas phase, it is likely that such deformation takes place to some extent in nonpolar solvents. However, the open-shell (triplet) CS states derived from the **1′** and **2′** are too large for structure optimization by the UHF methods. Furthermore, the effects of solvation should be taken into account to predict the reliable structures in each solvent. Here, we use the d_{cc} values of **1′** (14 Å) and **2′** (18 Å) for discussion of the Coulombic interactions in polar solvents, the magnitudes of the exchange and dipolar interactions ($|J|$ and $|D_{ZFS}|$) between the unpaired electrons in the CS states, and the electronic coupling on the ET energy surfaces ($|V|$).

As a model of the NI−R• part in **1R•** and **2R•**, the structure optimization of **3′R•** was carried out at the UHF/6-31+G* level. The distance between the center of the naphthalene plane in NI′ and the midpoint of the N−O bond in R•, was calculated to be 8.44 Å.

3.2. Free Energy Changes and Reaction Rates for the ET Processes. *(a) CS Processes from ^{1}ZP*.* The free energy changes (ΔG^S_{CS}) accompanying the CS processes from ^{1}ZP* were estimated for **1** and **2** from the Rehm−Weller relationship[35] and listed in Table 1. This table shows that these CS processes was exergonic for both **1** and **2** in PenOAc, THF, PrCN, and MeCN. The ΔG^S_{CS} values of **2** were more negative than the corresponding values of **1**, because the reduction potential of the NI part in **2** was by 0.12 V less negative than that in **1** due to the electron-withdrawing effect of the directly linked pyromellitdiimide (PI) group.[22] The ΔG^S_{CS} values for **1R•** and **2R•** were the same as the corresponding values for **1** and **2**, respectively, for the reduction potentials of the NI parts were not changed by substitution of the *n*-hexyl group by TEMPO-4-yl. Calculation from the Rehm−Weller equation would give positive ΔG^S_{CS} values for **1** and **2** in benzene or dioxane. However, this equation, which is based on the dielectric continuum model of solvation, sometimes underestimates solvation energies of charged solutes in nondipolar solvents. The CS states in benzene and dioxane can be stabilized by the quadrupolar interactions between the solvent molecules and charged centers.[25,36] The oxygen atoms in dioxane may also contribute to stabilization of the ZP$^{\bullet+}$ part through coordination to zinc at the axial positions. As was mentioned in section 3.1, the distance between ZP$^{\bullet+}$ and NI$^{\bullet-}$ may be reduced compared to the d_{cc} value to enhance the electrostatic interaction. Although the ΔG^S_{CS} values could not be obtained, the large k^S_{CS} values suggested that the CS processes from ^{1}ZP* should be exergonic in these solvents.

Although the d_{cc} value and the number of the intervening bonds between ZP and NI for **2** are larger than those for **1**, the k^S_{CS} values of **2** were comparable to those of **1**, as shown in Table 1. It is likely that the CS process from ^{1}ZP* in **2** took place through the sequential two-step reaction shown by eq 4 in polar solvents such as THF and PrCN, because the ΔG^S_{CS} value for ET from ^{1}ZP* to B_2 was predicted to be negative (Table 1)

$$^1\text{ZP}^*-\text{B}_2-\text{NI} \rightarrow {}^1[\text{ZP}^{\bullet+}-\text{B}_2^{\bullet-}-\text{NI}] \rightarrow {}^1[\text{ZP}^{\bullet+}-\text{B}_2-\text{NI}^{\bullet-}] \quad (4)$$

In model compounds mimicking the photosynthetic reaction center, PI has been used as a primary electron acceptor that received an electron from the excited donor and then gave the electron to a secondary acceptor such as quinone.[22,37,38] Wiederrecht et al. reported that the intramolecular charge shift from the radical anion of the PI moiety to the linked NI part took place in picosecond time scale.[22] On our apparatus with nanosecond time resolution, no transient absorption band assignable to $B_2^{\bullet-}$ was observed, but the absorption bands characteristic of NI$^{\bullet-}$ appeared instantaneously upon excitation. These facts suggest that the secondary charge shift in reaction 4 should be faster than the primary CS, and that the obtained k^S_{CS} values represent the ET rates from ^{1}ZP* to B_2. The driving force ($-\Delta G^S_{CS}$ in Table 1) of ET from ^{1}ZP* to B_2 in **2** was by (18−19) kJ mol^{-1} smaller than that from ^{1}ZP* to NI in **1**, whereas the ET distance of the former was shorter than the latter (Table 3). The similarity in the k^S_{CS} value of **1** and **2** probably results from these two competing factors. Because of the short lifetime and a large magnitude of *J*, the conversion from $^1[\text{ZP}^{\bullet+}-\text{B}_2^{\bullet-}-\text{NI}]$ to $^3[\text{ZP}^{\bullet+}-\text{B}_2^{\bullet-}-\text{NI}]$ can be neglected. In solvents of lower polarity, the long-distance ET from ^{1}ZP* to

NI may occur via super-exchange mechanism because the energy level of $^1[ZP^{\bullet+}-B_2^{\bullet-}-NI]$ is considered to be higher than that of $^1ZP^*-B_2-NI$. The mechanism of long-distance ET is a hot topic in ET chemistry, especially in biological systems such as CS in photosynthesis reaction centers and DNA-mediated charge transport.[39] In some cases, the sequential ET can dominate over the super-exchange pathway even if formation of the intermediate state is slightly endothermic.[40] As an alternative interpretation, the two mechanisms may be considered as the limiting cases in a framework of unified theory.[41] To understand the CS process of **2** in more detail, one need to study the formation kinetics of the CS state and its temperature dependence in picosecond time region, which seems beyond the scope of this paper. Whichever mechanism is valid, it should be noted that $^1[ZP^{\bullet+}-B_2-NI^{\bullet-}]$ was rapidly (<1ns) generated with a high efficiency.

(b) CS Processes from $^3ZP^*$. Excitation of **1** in PenOAc, THF, PrCN or MeCN gave the triplet CS state, $^3[ZP^{\bullet+}-B_1-NI^{\bullet-}]$, through ET from $^3ZP^*$ to NI (process **g** in Scheme 1b). The rate constant (k^T_{CS}) in MeCN was determined to be 1.4×10^7 s^{-1}, which was by 2 orders of magnitude smaller than k^S_{CS} (ca. 4×10^9 s^{-1}). This decrease in the ET rate can be attributed to the smaller driving force, as is seen in Table 1. Here, the triplet excitation energy (E_T) of ZP in **1** and **2** was assumed to be the same as that of Zn(ttp) (150 kJ mol^{-1}).[24c,42] Because the deactivation of $^3ZP^*-B_1-NI$ to the ground state is quite slow (The lifetimes of ^{3}Zn(ttp)* were reported to be 40 and 1500 μs in toluene and DMSO, respectively, at room temperature),[24b] the most part of $^3ZP^*-B_1-NI$ gave $^3[ZP^{\bullet+}-B_1-NI^{\bullet-}]$, even though the k^T_{CS} value was not so high.

In benzene and dioxane, $^3ZP^*$ was not quenched through the CS process for either **1** or **2**. On the contrary, the CS state derived from **2** gave $^3ZP^*-B_2-NI$ through CR in the triplet manifold (process **f** in Scheme 1a). These results indicate that $[ZP^{\bullet+}-B-NI^{\bullet-}]$ has a higher energy than $^3ZP^*-B-NI$. Thus, the energy levels of the CS states of **1** and **2** in these solvents were determined to be in a range of $-200 < \Delta G^S_{CR} < -150$ kJ mol^{-1}.

(c) CR Processes Leading to the Ground States. Upon excitation of **1** in benzene, the transient absorption bands assignable to $[ZP^{\bullet+}-B_1-NI^{\bullet-}]$ decayed within the duration of the laser pulse (<20 ns). As will be discussed in section 3.3, $[ZP^{\bullet+}-B_1-NI^{\bullet-}]$ born in the $|S\rangle$ state decays exclusively through CR to the ground state (process **d**) because the $|S\rangle \rightarrow |T\rangle$ conversion (process **e**) is much slower. In the other solvents, no transient absorption due to this singlet CS state was observed, although the Φ^S_{CS} values were almost the same as that in benzene. This result indicates that k^S_{CR} may be larger than k^S_{CS} in the solvents except for benzene. For similar porphyrin−diimide dyads with $d_{cc} = 13$ Å and $\Delta G^S_{CR} = -158$ kJ mol^{-1} in THF, the k^S_{CR} values were reported to be $(1.0-1.4) \times 10^{10}$ s^{-1}.[21a,38] From these facts, it can be estimated that $k^S_{CR} \geq 10^{10}$ s^{-1} for **1**.

In the case of **2**, $[ZP^{\bullet+}-B_2-NI^{\bullet-}]$ in the $|S\rangle$ state decayed through CR leading to the ground state (process **d**) and the spin conversion to the $|T\rangle$ state (process **e**). The k^S_{CR} values of 3.3×10^7 and 5.6×10^7 s^{-1} in PenOAc and THF, respectively (Table 2), were much smaller than the corresponding k^S_{CS} values (5.8×10^9 and 6.1×10^9 s^{-1}). According to the Marcus theory of nonadiabatic ET rates,[43] k^S_{CR} is estimated by eq 5

$$k^S_{CR} = (2\pi/h)\,|V|^2\,(\pi/\lambda k_B T)^{1/2} \exp[-(\Delta G^S_{CR} + \lambda)^2/4\lambda k_B T] \quad (5)$$

where V is the matrix element of the electronic coupling, and λ is the total reorganization energy. In contrast to the CS process from $^1ZP^*-B_2-NI$, B_2 (the bridging PI) cannot act as a good mediator for the CR process, because $[ZP^{\bullet+}-B_2^{\bullet-}-NI]$ state has much higher energy than $[ZP^{\bullet+}-B_2-NI^{\bullet-}]$. This CR process for **2** became faster with increase in the solvent polarity from benzene to PrCN. This solvent dependence is typical of ET reaction in the inverted region, and has been observed in CR processes of similar porphyrin−acceptor dyads.[43] The corresponding CR process for **1** lies also in the inverted region except for that in PrCN or MeCN.[45−47]

TABLE 4: *g*-Factors and HFC Constants of Radicals Derived from 1, 1R•, and 3R•, and Model Compounds in MeCN at Room Temperature

radical	*g*-factor	HFC constants/mT	$\lvert A_{HFC}\rvert^{b,c}$
$Zn(ttp)^{\bullet+}$ [a]	2.0027	0.149 (4N), 0.029 (8H), 0.044 (20H), 0.010 (8H)	0.46
$Zn(ttp)^{\bullet+}$	2.0026		
$ZP^{\bullet+}-B_1-NI$ (**1**$^{\bullet+}$)	2.0027		
$ZP-B_1-NI-R\bullet$ (**1R•**)	2.0063	1.577 (1N)	2.23
$ZP^{\bullet+}-B_1-NI-R\bullet$ (**1R**$^{\bullet\bullet+}$)	2.0026 2.0063	1.577 (IN)	
$NI-R\bullet$ (**3R•**)	2.0062	1.580 (1N)	2.23
$NI^{\bullet-}-R\bullet$	2.0050	0.79 (1N)	
$NI^{\bullet-}-RH$	2.0038	0.0935 (2N), 0.188 (4H), 0.022 (2H), 0.021 (1H)	0.38
$C_6NI^{\bullet-}$	2.0038	0.0965 (2N), 0.189 (4H), 0.016 (4H)	0.38

[a] In CH_2Cl_2 at 203 K. Determined by ESR, ENDOR, TRIPLE resonance techniques. ref 75. [b] Unit: mT. [c] ref 56.

3.3. Electron Spin−Spin Interactions in the CS States. *(a) Interactions between $NI^{\bullet-}$ and R•.* To obtain information on the spin−spin interactions between $NI^{\bullet-}$ and R• in $[ZP^{\bullet+}-B-NI^{\bullet-}-R\bullet]$, we measured the EPR spectrum of $NI^{\bullet-}-R\bullet$ which was prepared by reduction of **3R•** in MeCN. From the separation between the outermost lines observed at 77 K, the magnitude of the dipole−dipole interaction ($|D_{ZFS}|/g\beta$) was determined to be 5.3 mT. The distance between the center of the NI part and the midpoint of the nitroxide N−O bond was calculated to be 8.44 Å for the model compound **3′R•** (see section 3.1). In the point dipole approximation with this inter-radical distance, the $|D_{ZFS}|/g\beta$ value was estimated to be 4.64 mT. In the point charge approximation with the spin densities of the $NI^{\bullet-}$ part calculated by the DFT methods (See Experimental), the $|D_{ZFS}|/g\beta$ value was estimated to be 5.39 mT, which was in a good agreement with the observed value. The $|D_{ZFS}|/g\beta$ value of $NI^{\bullet-}-R\bullet$ was similar to that (4.4−9.3 mT) of the biradical anions employed in the previous study.[18a,19a,19b]

The *g*-factors and HFC constants of **3R•** and its reduced species are listed in Table 4. In the EPR spectrum measured at room temperature for the partially reduced sample of **3R•**, the two peaks assignable to the $m_N = \pm 1$ lines of $NI^{\bullet-}-R\bullet$ were observed, whereas its $m_N = 0$ line was overlapped with the signal of **3R•**. As shown in Table 4, the a_N value (0.79 mT) of $NI^{\bullet-}-R\bullet$ was a half of that of **3R•** (1.58 mT), and the *g*-factor (2.0050) was the average of those of **3R•** (2.0062) and $NI^{\bullet-}-R'$ (2.0038). Each line of the three-line signal of $NI^{\bullet-}-R\bullet$ was broader than that of **3R•**, probably due to the unresolved HFC with the N and H nuclei in the NI part. These magnetic properties indicate that $NI^{\bullet-}$ and R• are strongly coupled in $NI^{\bullet-}-R\bullet$ through the exchange interaction whose magnitude is much larger than the $|a_N|$ value of **3R•**.[48] Neither the sign nor magnitude of J for $NI^{\bullet-}-R\bullet$ could be determined experimentally.

For a variety of stable biradicals, the J values have been reported.[49−51] Most of them are conjugated systems in which two radical units are linked to each other with an aromatic coupler.[50] It is likely that the J value of such a conjugated

biradical is quite different from that of $NI^{\bullet-}-R\bullet$, even if the inter-radical distances are similar. As for TEMPO-linked biradical ions, Sugimoto et al. reported that the biradical cation of 2-[*N*-(TEMPO-4-yl)iminomethyl]tetrathiafulvalene has $J/g\beta = -5.6$ T (The negative sign means that the ground state is singlet) and $|D_{ZFS}|/g\beta = 1.62$ mT (This corresponds to the inter-radical distance of ca. 12 Å in the point dipole approximation).[51a] The $|J|/g\beta$ value of $NI^{\bullet-}-R\bullet$ may be larger than the highest B (1.7 T) applied in this study.

(b) Interactions between $ZP^{\bullet+}$ and $NI^{\bullet-}$. The magnitude of J for $[ZP^{\bullet+}-B_1-NI^{\bullet-}]$ was determined to be $|J|/g\beta = 0.45$ T in THF and PenOAc from the observed $R(B)$ vs B plots shown in Figure 4a.[52] According to the perturbation theory,[53] the J value due to the charge-transfer interaction for the CS state can be estimated by eq 6

$$J = -|V|^2/(\Delta G^{S}_{CR} + \lambda) \quad (6)$$

As the solvent polarity increases from benzene to MeCN, the $(\Delta G^{S}_{CR} + \lambda)$ value for **1** increases from negative to positive.[45,54] Equation 6 predicts that the sign of J for $[ZP^{\bullet+}-B_1-NI^{\bullet-}]$ is positive in benzene, dioxane, PenOAc, or THF, whereas it is negative in PrCN or MeCN. If $|V|$ were independent of the solvent properties, the $|J|$ value would be smaller in PenOAc than in THF. The observed $|J|$ values, however, were the same in these solvents. This discrepancy[55] may be attributed to the solvent-dependent distribution of the conformers different $|V|$ values. As was mentioned in Section 3.1, there can exist more than one conformers of $[ZP^{\bullet+}-B_1-NI^{\bullet-}]$ with different d_{cc} values. With decreasing solvent polarity, the conformer with the smaller d_{cc} value probably becomes more populated, and therefore, the averaged $|V|$ value increases. Alternatively, the relative contribution to J from the different coupling modes (through-bonds, through space, and through solvent) may be varied with the solvent properties. Although the $|J|$ value could not be determined in other solvents, it may be different from that observed in PenOAc and THF.

For the long-distance CS state $[ZP^{\bullet+}-B_2-NI^{\bullet-}]$ generated from **2**, the observed MFEs on the decay rates suggested that the HFC-induced $|S\rangle \leftrightarrow |T\rangle$ conversion efficiently took place under a zero field. This means that the $|J|$ value for this CS state was negligibly small. In general, the J value shows the exponential dependence on the inter-radical distance (R), as represented by $J(R) = J_0 \exp(-\alpha R)$. The k^{S}_{CR} value also shows the exponential dependence on R, $k^{S}_{CR}(R) = k^{S}_{CR}(0) \exp(-\beta R)$. Comparison of eq 5 and eq 6 indicates that both k^{S}_{CR} and J are proportional to $|V|^2$ and that their R dependence mainly originate from that of $|V|$. The k^{S}_{CR} values of **2** observed in PenOAc and THF were ~1/300−1/200 of the estimated k^{S}_{CR} value of **1**. If the α and β values are assumed to be equal, the J value for $[ZP^{\bullet+}-B_2-NI^{\bullet-}]$ is estimated to be ~2 mT. Alternatively, from the difference (4.6 Å) in the calculated d_{cc} value between anti-**1′** and **2′** (Table 3) and a typical α value of 1 $Å^{-1}$, it was evaluated to be ~4.5 mT. This range of the $|J|$ value is somewhat larger than the magnitude of the effective HFC interactions ($B_{1/2} = 0.84$ mT).[56]

As for the dipole−dipole interactions, the $|D_{ZFS}|/g\beta$ values were estimated to be 1.0 and 0.48 mT for $^3[ZP^{\bullet+}-B_1-NI^{\bullet-}]$ and $^3[ZP^{\bullet+}-B_2-NI^{\bullet-}]$, respectively, in the point dipole approximation with the inter-radical distances of 14 and 18 Å. These $|D_{ZFS}|/g\beta$ values are similar to the $B_{1/2}$ value. It is likely that the dipole−dipole interaction in $[ZP^{\bullet+}-B_1-NI^{\bullet-}]$ significantly contributes to the spin relaxation during the decay of the triplet CS state.

TABLE 5: Magnitudes of the Magnetic Interactions in the CS States[a]

interaction	$[ZP^{\bullet+}-B_1-NI^{\bullet-}]$	$[ZP^{\bullet+}-B_2-NI^{\bullet-}]$	$[ZP^{\bullet+}-B-NI^{\bullet-}-R\bullet]$
$\|J\|/g\beta$	450[b]	−[c]	$\|J(NI^{\bullet-}, R\bullet)\| \gg \|J(ZP^{\bullet+}, NI^{\bullet-})\|$ $\|J(NI^{\bullet-}, R\bullet)\| \gg \|J(ZP^{\bullet+}, NI^{\bullet-})\|$
$\|D_{ZFS}\|/g\beta$	1.0	0.47	$\|D_{ZFS}\ (NI^{\bullet-}, R\bullet)\| = 5.3$ $\|D_{ZFS}\ (ZP^{\bullet+}, R\bullet)\| \sim 0$
$B_{1/2}$[d,e]	0.84	0.84	
$\|\Delta gB\|$ ($B = 1.7$ T)	1.1	1.1	3.9 [f]

[a] Unit: mT. [b] In PenOAc and THF. [c] Estimated to be a few mT. See text in Section 3.3(b). [d] Ref 56. [e] The $|A_{HFC}|$ values of the individual radicals are given in Table 4. [f] $\Delta g = g(NI^{\bullet-}-R\bullet) - g(ZP^{\bullet+})$.

(c) Interactions between $ZP^{\bullet+}$ and R•. Because $ZP^{\bullet+}$ and R• in $[ZP^{\bullet+}-B-NI^{\bullet-}-R\bullet]$ are apart from each other, the spin−spin interactions between these two radical centers are expected to be much smaller than the other interactions operating for each of them. To confirm this assumption, the EPR spectrum of $[ZP^{\bullet+}-B_1-NI-R\bullet]$ was measured in MeCN at room temperature. Two signals were observed in $g \approx 2$ region. One of them was almost identical to the signal of $ZP-B_1-NI-R\bullet$, whereas the other showed a g-factor and a half-width quite similar to the corresponding values for the signal of $Zn(ttp)^{\bullet+}$ (Table 4). These results indicated that the $|J|$ value between $ZP^{\bullet+}$ and R• in $[ZP^{\bullet+}-B_1-NI-R\bullet]$ is smaller than the a_N values in these radicals. In $[ZP^{\bullet+}-B_2-NI-R\bullet]$ derived from **2R•**, the inter-radical distance between $ZP^{\bullet+}$ and R• is longer than that in $[ZP^{\bullet+}-B_1-NI-R\bullet]$, and therefore, the $|J|$ value should be smaller. Table 5 summarizes the magnitudes of the magnetic interactions which can induce the spin conversion of the CS states. The $|J|$ value of $NI^{\bullet-}-R\bullet$ pair is probably much larger than that of $ZP^{\bullet+}-NI^{\bullet-}$ or $ZP^{\bullet+}-R\bullet$ pair.[57]

3.4. Decay Dynamics of the CS States Derived from 1 and 1R•. *(a) Solvent Effects on the Decay Rate of $^3[ZP^{\bullet+}-B_1-NI^{\bullet-}]$.* Upon excitation of **1** in solvents of medium or high polarity, $^3[ZP^{\bullet+}-B_1-NI^{\bullet-}]$ was formed from CS from $^3ZP^*$. Because the $|T\rangle \rightarrow |S\rangle$ conversion was much slower than CR from the $|S\rangle$ state ($k^{S}_{CR} \geq 10^{10}\ s^{-1}$), the decay dynamics of $^3[ZP^{\bullet+}-B_1-NI^{\bullet-}]$ was governed by the spin conversion process. The efficiency of the $|T\rangle \rightarrow |S\rangle$ conversion depends on the J value, which can be varied with the solvent properties. As shown in Figure 2, the decay of the $\Delta A_{470}(t)$ curve for **1** increased with increase in solvent polarity from PenOAc to MeCN. Such solvent dependence seems contradictory in the following points: (i) Despite the same $|J|$ value, the $\Delta A_{470}(t)$ curve observed in THF decayed faster than in PenOAc. (ii) The B dependence of $R(B)$ shown in Figure 4a suggested that the $|J|$ value may be larger in PrCN or MeCN than in PenOAc or THF. The larger $|J|$ value should bring about the less efficient $|T\rangle \rightarrow |S\rangle$ conversion under a zero field. Contrary to this prediction, the decay of the $\Delta A_{470}(t)$ curve was faster in PrCN or MeCN than in THF or PenOAc.

These discrepancies may be explained as follows: As for (i), because the HFC-induced $|T\rangle \rightarrow |S\rangle$ conversion is inefficient as described above, the spin−lattice relaxation also has significant contribution to the decay of the $|T\rangle$ state. The relaxation rate (k_{rlx}) is varied with the correlation times of the fluctuating magnetic interactions,[7−9] which depend on the solvent viscosity. Among the solvents employed here, the viscosity at 293 K increases in the following order: MeCN (0.36 cP) < THF (0.575 cP) < PrCN (0.59 cP) < PenOAc (0.924 cP).[58] The longer correlation time in PenOAc may cause the smaller k_{rlx} value. Alternatively, in solvents of medium polarity such as PenOAc, the energy level of $^3[ZP^{\bullet+}-B_1-NI^{\bullet-}]$ is close to that of $^3ZP^*-$

B_1−NI. Therefore, an equilibrium may be attained between these two species. In the transient absorption spectrum measured at 1.8 μs after excitation of **1** in PenOAc, a broad band around 450 nm assignable to the T−T absorption of ^{3}ZP*−B_1−NI was observed as well as the sharp band at 470 nm due to the absorption of NI$^{\bullet-}$. Because the deactivation of ^{3}ZP*−B_1−NI to the ground state is much slower than the decay of the CS state, such equilibration lengthens the apparent lifetime of the CS state. With respect to (ii), the spin−orbit coupling (SOC)-induced CR process of ^{3}[ZP$^{\bullet+}$−B_1−NI$^{\bullet-}$] to give the singlet ground state (process **h** in Scheme 1b) and/or other nonspin selective reactions of the CS state may take place in PrCN and MeCN. For polymethylene-bridged zinc porphyrin−viologen dyads, it was reported that the SOC-induced back ET from the triplet RIP to the singlet ground states takes place at a rate of $k_{SOC} \approx 10^5$ s^{-1} and that this rate constant tends to increase with decrease in the inter-radical distance.[59,60] The magnitude of the SOC interaction for [ZP$^{\bullet+}$−B_1−NI$^{\bullet-}$] is likely to be insensitive to the nature of solvent. On the other hand, the Franck−Condon factor increases with increase in solvent polarity, as the case of the spin-allowed CR process from the singlet CS state, and therefore this SOC-induced process can have nonnegligible contribution to the decay of the triplet CS state in polar solvents, especially when the spin relaxation is slow. Thus, the solvent dependence of the decay rate of [ZP$^{\bullet+}$−B_1−NI$^{\bullet-}$] did not result from one dominant factor but from combination of several factors.

(b) Spin Dynamics of [ZP$^{\bullet+}$−B_1−$A^{\bullet-}$−R•]. Upon excitation of **1R•** in benzene or dioxane, the transient absorption bands assigned to the CS state had decayed within the duration of the laser pulse. This result indicated that the spin-allowed CR to give the ground state (process **d** in Scheme 1c) was faster than the spin conversion. Such instantaneous decay of the CS state was also observed for **1**. Thus, the spin effects on the decay dynamics of the CS state could not be clarified in these solvents.

On excitation of **1R•** in solvents of medium or high polarity, the CS process from ^{3}ZP* gave [ZP$^{\bullet+}$−B_1−NI$^{\bullet-}$−R•] in either the doublet (|D⟩) or quartet (|Q⟩) state in the statistical ratio of 1:2 (process **g** in Scheme 1d). According to the spin catalysis theory of Buchachenko and Berdinsky,[61] the |D⟩ ↔ |D′⟩ mixing should be efficient for three-spin systems with largely different J values such as [ZP$^{\bullet+}$−B_1−NI$^{\bullet-}$−R•] (Table 5). It was, therefore, expected that [ZP$^{\bullet+}$−B_1−NI$^{\bullet-}$−R•] born in the |D⟩ state decayed faster than that born in the |Q⟩ state. However, the $\Delta A_{470}(t)$ curve observed for **1R•** under a zero field was almost fit to a single-exponential function. This kinetic behavior can be explained as follows: Under the condition that $k_{DD'}$, $k^S_{CR} \gg k_{DQ}$, the population of the |D⟩ state is too low to contribute the transient absorbance, and the observed $\Delta A_{470}(t)$ curve mainly represents the kinetic behavior of the |Q⟩ state. The energy gap between the |Q⟩ and |D⟩ states is determined by the J values between two radical centers in the three-spin system.[61] If this gap is as small as $|A_{HFC}|$, the HFC-induced conversion between the |Q⟩ and the |D⟩ or |D′⟩ state efficiently takes place,[61d,62,63] whereas with a larger gap the electron spin dipole−dipole interaction plays an important role in the |Q⟩ → |D⟩ conversion.[61,62,64] As seen in Figure 3, ^{4}[ZP$^{\bullet+}$−B_1−NI$^{\bullet-}$−R•] decayed much faster than ^{3}[ZP$^{\bullet+}$−B_1−NI$^{\bullet-}$]. The decay rates of **1** and **1R•** listed in Table 2 correspond to the total decay rates of [ZP$^{\bullet+}$−B_1−NI$^{\bullet-}$(−R•)] in the |T⟩ or |Q⟩ states, which include the |T⟩ → |S⟩ or |Q⟩ → |D⟩ spin conversion rate and the contribution from any other decay processes. The insensitivity of the decay rate of ^{4}[ZP$^{\bullet+}$−B_1−NI$^{\bullet-}$−R•] to the solvent properties suggested that the major contribution to the observed rate should be ascribed to the |Q⟩ → |D⟩ conversion rate (k_{DQ}). In the case of ^{3}[ZP$^{\bullet+}$−B_1−NI$^{\bullet-}$], the SOC-induced CR reaction also took place, especially in polar solvents such as PrCN and MeCN, as was described in section 3.4(a). These results indicate that the |Q⟩ → |D⟩ conversion of ^{4}[ZP$^{\bullet+}$−B_1−NI$^{\bullet-}$−R•] is more efficient than the |T⟩ → |S⟩ conversion of ^{3}[ZP$^{\bullet+}$−B_1−NI].

As for the MFEs on the decay of [ZP$^{\bullet+}$−B_1−NI$^{\bullet-}$−R•], the $R(B)$ value increased with increasing B from 0 to 1 T, and the MFEs were saturated at $B = 1$ T (Figure 4b). Such B dependence of the $R(B)$ value was quite similar to that previously observed for the free ion yield from the biradical−radical ion pair born in the |Q⟩ state.[19b] In the previous case, we employed the biradical anion of *N*-hexyl-*N*′-(TEMPO-4-yl)-pyromellitdiimide (PI$^{\bullet-}$−R•), for which the estimated inter-radical distance (8.6 Å) was similar to that for NI$^{\bullet-}$−R• (8.44 Å). The J values between the radical anion part and R• may be also similar for these two systems. On the basis of this analogy, the MFEs observed for **1R•** can be explained by the relaxation mechanism (RM) for triplet−doublet pairs.[64] As shown in Scheme 2c, the four sublevels of the |Q⟩ state are converted to the |D⟩ state with a rate of k_{DQ} under a zero field. Under high magnetic fields ($B \gg |D_{ZFS}|/g\beta$), the $|Q_{\pm3/2}\rangle$ sublevels are energetically separated from the $|D_{\pm1/2}\rangle$ or $|Q_{\pm1/2}\rangle$ sublevels. The interconversion between such nondegenerate sublevels takes place through the spin relaxation induced mainly by the electron spin dipole−dipole interaction between NI$^{\bullet-}$ and R•. The biphasic decay of the $\Delta A_{470}(t)$ curves observed under $B = 0.1$ T (Figure 3b) can be explained by the existence of the faster-decaying $|Q_{\pm1/2}\rangle$ sublevels and the slower-decaying $|Q_{\pm3/2}\rangle$ ones. With increasing B, the relaxation rate monotonically decreases to an asymptotic value.[64] As a result, the lifetime of the $|Q_{\pm3/2}\rangle$ sublevels increases, whereas that of the $|Q_{\pm1/2}\rangle$ ones is substantially unchanged. This is consistent with the observation that the increasing B decelerated the decay of the slower-decaying component without significant effects on the faster-decaying one (Figure 3b).

3.5. Spin Dynamics of the CS States Derived from 2 and 2R•. *(a) In Benzene and Dioxane.* The MFEs on $R(B)$ (i.e., relative yield of ^{3}ZP*−B_2−NI) observed for **2** in benzene and dioxane can be explained as follows: The decrease in $R(B)$ with increasing B from 0 to 0.1 T is attributable to the hyperfine coupling mechanism (HFCM).[7,8] Under a zero field, [ZP$^{\bullet+}$−B_2−NI$^{\bullet-}$] born in the |S⟩ state is converted to the three sublevels of |T⟩ state through the HFC-induced spin conversion in competition with CR leading to the ground state. Under magnetic fields much higher than $|A_{HFC}|$ and $|J|$, the |S⟩ ↔ $|T_0\rangle$ conversion still takes place, whereas the $|T_{\pm1}\rangle$ sublevels remain unpopulated because the |S⟩ ↔ $|T_{\pm1}\rangle$ and $|T_0\rangle$ ↔ $|T_{\pm1}\rangle$ relaxation is much slower than the decay of the |S⟩ state through CR. The increase in $R(B)$ with increasing B from 0.2 to 1.7 T can be explained in terms of the Δg mechanism (ΔgM).[7,8] According to this mechanism, the |S⟩ ↔ $|T_0\rangle$ conversion induced by the isotropic Zeeman interaction is accelerated with increasing B. As shown in Table 5, the magnitude of this interaction ($|\Delta g\beta B|$) at $B = 1.7$ T is similar to the magnitude of the effective HFC interaction ($g\beta B_{1/2}$). Thus, it seems reasonable that the MFEs due to both the mechanisms could be observed in the field range of 0−1.7 T.

In benzene or dioxane, the Φ_T value of **2R•** was higher than that of **2**. The presence of R• can affect the Φ_T value in the following ways: (i) ISC from ^{1}ZP* to ^{3}ZP* is enhanced,[26] (ii) ^{1}ZP* can be quenched by R• through other processes such as energy transfer,[26] (iii) the spin-allowed CR from ^{2}[ZP$^{\bullet+}$−B_2−NI$^{\bullet-}$−R•] in the |D⟩ state to give ^{2}[^{3}ZP*−B_2−NI−^{2}R•] is

opened, and (iv) the $|D\rangle \rightarrow |Q\rangle$ conversion of $[ZP^{\bullet+}-B_2-NI^{\bullet-}-R\bullet]$ is faster than the $|S\rangle \rightarrow |T\rangle$ conversion of $[ZP^{\bullet+}-B_2-NI^{\bullet-}]$. Factors (i), (iii), and (iv) increase the Φ_T value, whereas factor (ii) decreases it. The Φ_T (B) value for **2R•** can be expressed eq 7, which is a modified version of eq 3

$$\Phi_T(B) = (k_{ISC} + k^R_{ISC})/(k_{FL} + k_{nr} + k^R_{nr} + k_{ISC} + k^R_{ISC} + k^S_{CS}) + \Phi^D_{CS} \times \eta_T(B) \quad (7)$$

In the first term of eq 7, factors (i) and (ii) are taken into consideration. These quenching processes have probably only small contribution because of the large distance between ZP and R•.[28] Indeed, the estimated Φ^D_{CS} value (0.7) gives the upper limit of 0.3 for the first term of eq 7. The η_T (B) value in eq 7 reflects factors (iii) and (iv). The observed high Φ_T (0 T) value (0.85) and the lack of MFE for **2R•** indicated that k^T_{CR} and k_{DQ} are larger than k^S_{CR} in benzene. In dioxane, $[ZP^{\bullet+}-B_2-NI^{\bullet-}-R\bullet]$ decayed partially through CR leading to the ground state (process **d**) in competition with CR leading to $^3ZP^*-B_2-NI-R\bullet$, suggesting that k^S_{CR} value was larger in dioxane than in benzene and/or that the k^T_{CR} value was smaller in dioxane than in benzene. The observed MFEs on the $\Phi_T(B)$ value for **2R•** in dioxane can be explained by the decrease in the $|D\rangle \leftrightarrow |Q\rangle$ conversion efficiency with increasing B, as the MFEs observed for **1R•**.

(b) In Solvents of Medium or High Polarity. As seen in Figure 5b, the $\Delta A_{470}(t)$ curves observed for **2** in THF exhibited biphasic decay. Because the $|S\rangle$ state decayed through CR dominantly over the conversion to the $|T\rangle$ state (Table 2), the initial decaying part of the $\Delta A_{470}(t)$ curve mainly represents the time profile of the population of the $|S\rangle$ state generated by CS from $^1ZP^*-B_2-NI$. The B dependence of $R(B)$ for this component (Figure 6a) was similar to that observed in benzene or dioxane and can be explained by the HFCM and ΔgM. As was mentioned in section 3.3(b), the $|J|$ value of $[ZP^{\bullet+}-B_2-NI^{\bullet-}]$ is likely to be comparable to or somewhat larger than its $|A_{HFC}|$ value. Therefore, the efficiency of the $|S\rangle \leftrightarrow |T_0\rangle$ conversion is expected to be lower than the case of $|J| \ll |A_{HFC}|$.[7,8,65] Indeed, the effective[66] conversion rate (k_{ST}) of $(3-4) \times 10^6$ s^{-1} (Table 2) observed in PenOAc and THF is lower than the $|S\rangle \leftrightarrow |T_0\rangle$ oscillation frequency of 1.1×10^7 s^{-1} (or $\omega_{ST0} = 6.9 \times 10^7$ rad s^{-1}) evaluated from the $B_{1/2}$ value (Table 5) for the case of $|J| = 0$. In the $R(B)$ vs B plots shown in Figure 6a, no maximum due to the J-resonance was observed. Because of the small magnitude of $|J|$, broadening caused by plausible factors such as the nonzero-$|A_{HFC}|$ and the lifetime broadening easily obscured appearance of a maximum. In longer time region ($t \geq 800$ ns) the $R(B)$ value steeply increased with increasing B from 0 to 0.05 T, showed further gradual increase up to $B \approx 0.2$ T, and became almost constant under $0.2 \leq B \leq 1.7$ T (Figure 6b). This field-sensitive component is assigned to $[ZP^{\bullet+}-B_2-NI^{\bullet-}]$ in the $|T_{\pm1}\rangle$ sublevels, which is generated through the CS from $^3ZP^*-B_2-NI$. The observed MFEs can be explained by the HFCM in low fields and by the RM in higher fields.

The spin effects observed for **2R•** were similar to those observed for the previously studied three-spin CS state (referred to as $[PTZ^{\bullet+}-B_3-PI^{\bullet-}-R\bullet]$, where PTZ is the *N*-substituted phenothiazine and B_3 is 4,4′-dimethylene-1,1′-biphenyl).[18a] The characteristic features are (i) that the initial decay of the CS state generated from the singlet excited state of the donor ($^1ZP^*$ or $^1PTZ^*$) was retarded by the presence of R• and (ii) that the decay kinetics under a zero field was changed from double exponential for the two-spin systems to single exponential for the three-spin ones. These features result from the fact that the $|D\rangle$ state generated by the CS process of the three-spin system can be converted to the nonreactive state (that is, $|Q\rangle$ state) more efficiently than the $|S\rangle$ state of the corresponding two-spin CS state. The MFEs observed for **2R•** can be explained by the RM for triplet−doublet pairs, as was the case of **1R•**. As seen in Figure 6, B value at which the MFE reached saturation was higher for **2R•** than for **2** in either THF or PrCN. This difference can be attributed to the difference in mechanism: HFCM for **2** and RM for **2R•**.

Finally, let us compare the spin and magnetic field effects on the decay dynamics among $[ZP^{\bullet+}-B_1-NI^{\bullet-}-R\bullet]$, $[ZP^{\bullet+}-B_2-NI^{\bullet-}-R\bullet]$, and $[PTZ^{\bullet+}-B_3-PI^{\bullet-}-R\bullet]$. The latter two systems showed quite similar effects, as described above. On the other hand, the short-distance CS state $[ZP^{\bullet+}-B_1-NI^{\bullet-}-R\bullet]$ exhibited some different features such as the lack of the spin effect in benzene or dioxane. The plausible reason of this difference is that the CR rate (k^S_{CR}) of $[ZP^{\bullet+}-B_1-NI^{\bullet-}-R\bullet]$ is too large to allow competitive occurrence of the conversion to the $|Q\rangle$ states.

The $|J|$ value for the corresponding two-spin analogue increases in the following order: $[ZP^{\bullet+}-B_2-NI^{\bullet-}]$ (at most several mT) ≤ $[PTZ^{\bullet+}-B_3-PI^{\bullet-}]$ (3.75 mT in dioxane)[18a] < $[ZP^{\bullet+}-B_1-NI^{\bullet-}]$ (450 mT in PenOAc and THF). It is notable that the presence of R• can accelerate the interconversion between the spin states with different multiplicities, irrespective of the magnitude of J for the two-spin analogue. The energy splitting between the $|D\rangle$ and $|Q\rangle$ states may be dominantly governed by the J value between $NI^{\bullet-}$ (or $PI^{\bullet-}$) and R•. In these systems, the $|D\rangle \leftrightarrow |Q\rangle$ spin conversion is mainly induced by the electron spin dipole−dipole interaction between $NI^{\bullet-}$ (or $PI^{\bullet-}$) and R•. For these systems, the magnitude of $|J|$ and $|D_{ZFS}|$ between $NI^{\bullet-}$ (or $PI^{\bullet-}$) and R• are likely similar to each other, which may cause the observed similarities of the spin effects.

4. Conclusion

Photoexcitation of **1**, **1R•**, **2**, and **2R•** efficiently gave CS states $[ZP^{\bullet+}-B-NI^{\bullet-}(-R\bullet)]$ through intramolecular ET from $^1ZP^*$ to NI with rate constants (k^S_{CS}) of $(4-8) \times 10^9$ s^{-1} in various solvents. The energy level of the CS state was higher than that of $^3ZP^*$ in benzene and dioxane, while lower than $^3ZP^*$ in PenOAc, THF, PrCN, and MeCN. The CS states decayed through the CR processes to give $ZP-B-NI(-R\bullet)$ or $^3ZP^*-B-NI(-R\bullet)$. The presence of R• affected the decay processes of the CS state in the following two ways: (i) The energy gap between the $|D\rangle$ and $|Q\rangle$ states of $[ZP^{\bullet+}-B_1-NI^{\bullet-}-R\bullet]$ is different from that between the $|S\rangle$ and $|T\rangle$ states of $[ZP^{\bullet+}-B_1-NI^{\bullet-}]$. (ii) The dipole−dipole interaction between $NI^{\bullet-}$ and R• induces the effective $|D\rangle \leftrightarrow |Q\rangle$ conversion, and as a result $^4[ZP^{\bullet+}-B_1-NI^{\bullet-}-R\bullet]$ decayed much faster than $^3[ZP^{\bullet+}-B_1-NI^{\bullet-}]$.

For the long-distance CS state, $[ZP^{\bullet+}-B_2-NI^{\bullet-}]$, the k^S_{CR} value was much smaller than that of $[ZP^{\bullet+}-B_1-NI^{\bullet-}]$ due to the larger separation distance. The k^S_{CR} value increased with increasing solvent polarity from PenOAc to PrCN, indicating that this CR process was in the inverted region of the Marcus theory. The insertion of the PI unit diminished not only the k^S_{CR} value but also the $|J|$ value. Therefore, the HFC-induced $|S\rangle \leftrightarrow |T\rangle$ conversion of $[ZP^{\bullet+}-B_2-NI^{\bullet-}]$ took place in competition with the CR process. The decay kinetics of this CS state was also affected by R• by the same mechanism as the case of $[ZP^{\bullet+}-B_1-NI^{\bullet-}]$. Because the $|D\rangle \leftrightarrow |Q\rangle$ conversion was faster than the $|S\rangle \leftrightarrow |T\rangle$ one, the effects of R• were observed on the decay of $[ZP^{\bullet+}-B_2-NI^{\bullet-}]$ born in the $|S\rangle$ state especially in

early time region (typically from several nano- to several tens of nano-seconds). Such retardation of the initial decay of the CS state can be utilized to enhance any secondary reaction processes such as charge shift reactions.

5. Experimental Section

Materials. Benzene, THF, and MeCN were of spectroscopic grade and used as solvents for laser flash photolysis and fluorescence measurements without further purification. 1,4-Dioxane (Cica-Merck, HPLC grade) was passed through activated alumina just before use. PrCN was distilled and stored over molecular sieves 4A. PenOAc of analytical grade was used as received. For electrochemical studies and EPR measurements, dehydrated MeCN and CH_2Cl_2 (Organics) were used as received. Zn(tpp) and Zn(ttp) were prepared by metalation of the corresponding free bases with $Zn(OAc)_2$ in $CHCl_3$-MeOH.[21a] *N*,*N*′-Di-(*n*-hexyl)naphthalene-1,8:4,5-tetracarboxydiimide (C_6-NI) was obtained by the methods of Hamilton et al.[67] Synthetic procedures and ^{1}H NMR spectral data of **1**, **1R•**, **2**, **2R•**, and **3R•** are given in Supporting Information.

Fluorescence Spectra. The sample solutions ($\sim 3 \times 10^{-6}$ M) were deaerated by bubbling with argon gas presaturated with the corresponding solvents for 20 min before the measurements. The excitation wavelength was set to the maximum (550−556 nm) of the 0,1 transition of the Q-band, which was slightly dependent on the solvent but not on the identity of the compounds. The fluorescence spectra were recorded on a Shimadzu RF510 spectro-fluorometer equipped with a quantum counter at 293 K. The relative fluorescence quantum yields (Φ_{FL}/Φ^0_{FL}) were obtained from the integrated intensities in a wavelength range of 565−750 nm.

Laser Flash Photolyses. Each of the sample solutions (3 cm^3) was placed in a long-necked quartz cell ($10 \times 5 \times 45$ mm) and bubbled with argon gas presaturated with the corresponding solvents for 20 min before experiments. The sample concentration was $(1-2) \times 10^{-5}$ M. All the measurements were carried out at 293 K. The second (532 nm) harmonic of a Quanta-Ray GCR-103 Nd:YAG laser was used as excitation light. The transient signals were accumulated 10 times at the repetition rate of 0.6 Hz. The magnetic fields were generated by a Tokin SEE−10W electromagnet.

EPR Spectra. The EPR spectra were recorded with 100-kHz modulation on an X-band EPR spectrometer (JEOL, JES−RE1X). The magnetic field and the microwave frequency were determined with an NMR field meter (Echo Electronics, EFM-2000AX) and a microwave counter (Echo Electronics, EMC-14), respectively.

Reduction of **3R•** was carried out by shaking with 0.5% (w/w) Na−Hg in MeCN under vacuum at a low concentration (ca. 3×10^{-4} M) in the presence of 4,7,13,16,21,24-hexaoxa-1,10-diazabicyclo[8.8.8]hexacosane (0.04 M) to avoid ion-pairing with Na^+.[68] The progress of reduction was monitored by EPR spectral change at room temperature. When a sharp signal due to the two-electron reduced species appeared, the solution was separated from Na−Hg. The EPR spectrum of this solution, which contained unreduced **3R•** (NI−R•), one-electron reduced species (NI$^{\bullet-}$−R•), and two-electron reduced one (NI$^{\bullet-}$−RH), was immediately recorded at 77 K. The microwave power of 0.6 mW was used. A more intense microwave was applied for attempt to detect a signal due to the $\Delta m_S = 2$ transition, but no signal could be observed. The solution was warmed to room temperature and shaken again with Na−Hg until complete conversion to NI$^{\bullet-}$−RH was attained. The EPR spectrum of NI$^{\bullet-}$−RH was recorded at room temperature. The isotropic HFC constants of C_6NI$^{\bullet-}$ and NI$^{\bullet-}$−RH (Table 4) were determined by simulation with the software WIN SimFonia.[69]

Oxidation of **1R•** and Zn(ttp) was carried out by addition of a small aliquot of a stock solution of $Fe^{III}(ClO_4)_3$ in MeCN to the porphyrin solution in CH_2Cl_2 under air. In the case of **1R•**, the amount of $Fe^{III}(ClO_4)_3$ added was less than 1 equivalent to avoid oxidation of the TEMPO moiety. The EPR spectra were immediately measured at room temperature.

Quantum Chemical Calculations. Structure optimization of **1′** and **2′** was carried out at the Hartree−Fock (HF) level with the LanL2DZ[70] and 3-21G basis sets for zinc and the other elements, respectively. As for **3′R•** the optimization was carried out at UHF/6-31G level. To determine the spin densities of the radical anion of *N*,*N*′-dimethylnaphthalene-1,8:4,5-tetracarboxydiimide, the hybrid DFT calculations were carried out at the unrestricted B3LYP[71] level with the 6-31+G* basis sets. The calculated $|a_N|$ and $|a_H|$ values (0.096 and 0.187 mT, respectively) agreed well with the experimental values (0.0965 and 0.189 mT) obtained for C_6NI$^{\bullet-}$ (Table 4). These calculations were carried out with Gaussian 98 program[72] on a Fujitsu VPP700E supercomputer at RIKEN.

Acknowledgment. Y.M. thanks the financial supports from The Nishida Research Fund for Fundamental Organic Chemistry. This work was financially supported by a Grant-in-Aid (No. 12740332) from the Ministry of Education, Science, Sports and Culture, Japan.

Supporting Information Available: Synthetic procedures and ^{1}H NMR spectral data for **1**, **1R•**, **2**, **2R•**, and **3R•**; Observed transient absorption spectra upon excitation of **1** in MeCN and calculated component spectra; Some of observed $\Delta A(t)$ curves and curve-fitting. This material is available free of charge via the Internet at http://pubs.acs.org.

Appendix

The three-spin CS state [D$^{\bullet+}$−B−A$^{\bullet-}$−R•] has the four quartet ($|Q\rangle$) and four doublet ($|D'\rangle$ and $|D\rangle$) spin sublevels. In high field case, these sublevels are expressed in terms of the spin state of each radical, $|\alpha_i\rangle$ and $|\beta_i\rangle$ (i = D, A, and R), as follows[61e,73]

$$|Q_{+3/2}\rangle = |\alpha_D\rangle\,|\alpha_A\rangle\,|\alpha_R\rangle$$

$$|Q_{+1/2}\rangle = 3^{-1/2}\,(|\alpha_D\rangle\,|\alpha_A\rangle\,|\beta_R\rangle + |\alpha_D\rangle\,|\beta_A\rangle\,|\alpha_R\rangle + |\beta_D\rangle\,|\alpha_A\rangle\,|\alpha_R\rangle)$$

$$|Q_{-1/2}\rangle = 3^{-1/2}\,(|\beta_D\rangle\,|\beta_A\rangle\,|\alpha_R\rangle + |\beta_D\rangle\,|\alpha_A\rangle\,|\beta_R\rangle + |\alpha_D\rangle\,|\beta_A\rangle\,|\beta_R\rangle)$$

$$|Q_{-3/2}\rangle = |\beta_D\rangle\,|\beta_A\rangle\,|\beta_R\rangle$$

$$|D_{+1/2}\rangle = 6^{-1/2}\,(2|\alpha_D\rangle\,|\alpha_A\rangle\,|\beta_R\rangle - |\alpha_D\rangle\,|\beta_A\rangle\,|\alpha_R\rangle - |\beta_D\rangle\,|\alpha_A\rangle\,|\alpha_R\rangle)$$

$$|D_{-1/2}\rangle = 6^{-1/2}\,(2|\beta_D\rangle\,|\beta_A\rangle\,|\alpha_R\rangle - |\beta_D\rangle\,|\alpha_A\rangle\,|\beta_R\rangle - |\alpha_D\rangle\,|\beta_A\rangle\,|\beta_R\rangle)$$

$$|D'_{+1/2}\rangle = 2^{-1/2}\,(|\alpha_D\rangle\,|\beta_A\rangle\,|\alpha_R\rangle - |\beta_D\rangle\,|\alpha_A\rangle\,|\alpha_R\rangle)$$

$$|D'_{-1/2}\rangle = 2^{-1/2}\,(|\alpha_D\rangle\,|\beta_A\rangle\,|\beta_R\rangle - |\beta_D\rangle\,|\alpha_A\rangle\,|\beta_R\rangle)$$

References and Notes

(1) Wasielewski, M. R. *Chem. Rev.* **1992**, *92*, 435.
(2) (a) Gust, D.; Moore, T. A.; Moore, A. L. *Acc. Chem. Res.* **1993**, *26*, 198. (b) Gust, D.; Moore, T. A.; Moore, A. L. *Acc. Chem. Res.* **2001**, *34*, 40.

(3) (a) Luo, C.; Guldi, D. M.; Imahori, H.; Tamaki, K.; Sakata, Y. *J. Am. Chem. Soc*. **2000**, *122*, 6535. (b) Tsue, H.; Imahori, H.; Kaneda, T.; Tanaka, Y.; Okada, T.; Tamaki, K.; Sakata, Y. *J. Am. Chem. Soc*. **2000**, *122*, 2279, and references therein. (c) Imahori, H.; Tamaki, K.; Guldi, D. M.; Luo, C.; Fujitsuka, M.; Ito, O.; Sakata, Y.; Fukuzumi, S. *J. Am. Chem. Soc*. **2001**, *123*, 2607.

(4) (a) Greenfield, S. R.; Svec, W. A.; Gosztola, D.; Wasielewski, M. R. *J. Am. Chem. Soc*. **1996**, *118*, 6767. (b) Liddell, P. A.; Kuciauskas, D.; Sumida, J. P.; Nash, B.; Nguyen, D.; Moore, A. L.; Moore, T. A.; Gust, D. *J. Am. Chem. Soc*. **1997**, *119*, 1400. (c) Tan, Q.; Kuciauskas, D.; Lin, S.; Stone, S.; Moore, A. L.; Moore, T. A.; Gust, D. *J. Phys. Chem. B* **1997**, *101*, 5214. (d) Carbonera, D.; Valentin, M. D.; Corvaja, C.; Agostini, G.; Giacometti, G.; Liddell, P. A.; Kuciauskas, D.; Moore, A. L.; Moore, T. A.; Gust, D. *J. Am. Chem. Soc*. **1998**, *120*, 4398. (e) Liddell, P. A.; Gerdenis, K.; de la Garza, L.; Bahr, J. L.; Moore, A. L.; Moore, T. A.; Gust, D. *Helv. Chim. Acta* **2001**, *84*, 2765.

(5) (a) Lukas, A. S.; Miller, S. E.; Wasielewski, M. R. *J. Phys. Chem. B* **2000**, *104*, 931. (b) Hayes, R. T.; Wasielewski, M. R.; Gosztola, D. *J. Am. Chem. Soc*. **2000**, *122*, 5563. (c) Miller, S. E.; Lukas, A. S.; Marsh, E.; Bushard, P.; Wasielewski, M. R. *J. Am. Chem. Soc*. **2000**, *122*, 7802. (d) Davis, W. B.; Ratner, M. A.; Wasielewski, M. R. *J. Am. Chem. Soc*. **2001**, *123*, 7877.

(6) Arimura, T.; Ide, S.; Suga, Y.; Nishioka, T.; Murata, S.; Tachiya, M.; Nagamura, T.; Inoue H. *J. Am. Chem. Soc*. **2001**, *123*, 10 744.

(7) (a) Hayashi, H. *Dynamic Spin Chemistry*; Nagakura, S.; Hayashi, H.; Azumi, T. Eds.; Kodansha-Wiley: Tokyo and New York, 1998; pp 7−47. (b) Hayashi, H.; Sakaguchi, Y.; Wakasa, M. *Bull. Chem. Soc. Jpn*. **2001**, *74*, 773.

(8) Steiner, U. E.; Ulrich, T. *Chem. Rev*. **1989**, *89*, 51.

(9) Fujiwara, Y.; Nakagaki, R.; Tanimoto, Y. *Dynamic Spin Chemistry*; Nagakura, S.; Hayashi, H.; Azumi, T. Eds.; Kodansha-Wiley: Tokyo and New York, 1998; pp 49−81.

(10) (a) Recently exceptionally large $|J|$ values have been observed in short-distance CS states. (b) Wegner, M.; Fischer, H.; Grosse, S.; Vieth, H.-M.; Oliver, A. M.; Paddon-Row: M. N. *Chem. Phys*. **2001**, *264*, 341.

(11) (a) Werner, U.; Sakaguchi, Y.; Hayashi, H.; Nohya, G.; Yoneshima, R.; Nakajima, S.; Osuka, A. *J. Phys. Chem*. **1995**, *99*, 13 930. (b) Klumpp, T.; Linsenmann, M.; Larson, S. L.; Limoges, B. R.; Bürssner, D.; Krissinel, E. B.; Elliot, C. M.; Steiner, U. E. *J. Am. Chem. Soc*. **1999**, *121*, 1076. (c) Kuciauskas, D.; Liddell, P. A.; Moore, A. L.; Gust, D. *J. Am. Chem. Soc*. **1998**, *120*, 10 880.

(12) (a) Sakaguchi, Y.; Hayashi, H. *J. Phys. Chem. A* **1997**, *101*, 549. (b) Shimada, E.; Nagano, M.; Iwahashi, M.; Mori, Y.; Sakaguchi, Y.; Hayashi, H. *J. Phys. Chem. A* **2001**, *105*, 2997.

(13) (a) Peters, K. S.; Lee, J. *J. Phys. Chem*. **1993**, *97*, 3761. (b) Aich, S.; Basu, S. *Chem. Phys. Lett*. **1997**, *281*, 247. (c) Hviid, L.; Brouwer, A. M.; Paddon-Row: M. N.; Verhoeven, J. W. *ChemPhysChem* **2001**, *2*, 232.

(14) (a) Burshtein, A. I.; Krissinel, E. *J. Phys. Chem. A* **1998**, *102*, 816. (b) Burshtein, A. I.; Sivachenko, A. Yu. *Chem. Phys*. **1998**, *235*, 257.

(15) (a) van Willigen, H.; Jones, G. II; Farahat, M. S. *J. Phys. Chem*. **1996**, *100*, 3312. (b) Weis, V.; van Willigen, H. *J. Porphyrins Phthalocyanines* **1998**, *2*, 353. (c) Bussandri, A.; van Willigen, H. *J. Phys. Chem. A* **2001**, *105*, 4669.

(16) (a) van der Est, A. J.; Fuechscle, G.; Stehlik, D.; Wasielewski, M. R. *Ber. Bunsen-Ges*. **1996**, *100*, 2081. (b) Levanon, H.; Galili, T.; Regev, A.; Wiederrecht, G. P.; Svec, W. A.; Wasielewski, *J. Am. Chem. Soc*. **1998**, *120*, 6366. (c) Kiefer, A. M.; Kast, S. M.; Wasielewski, M. R.; Laukenmann, K.; Kothe, G. *J. Am. Chem. Soc*. **1999**, *121*, 188. (d) Wiederrecht, G. P.; Svec, W. A.; Wasielewski, M. R.; Galili, T.; Levanon, H. *J. Am. Chem. Soc*. **1999**, *121*, 7726. (e) Wiederrecht, G. P.; Svec, W. A.; Wasielewski, M. R.; Galili, T.; Levanon, H. *J. Am. Chem. Soc*. **2000**, *122*, 9715.

(17) Fuhs, M.; Elger, G.; Osintsev, A.; Popov, A.; Kurreck, H.; Möbius, K. *Mol. Phys*. **2000**, *98*, 1025.

(18) (a) Mori, Y.; Sakaguchi, Y.; Hayashi, H. *Bull. Chem. Soc. Jpn*. **2001**, *74*, 293. (b) Conti et al. also reported the intramolecular photoinduced ET for donor-bridge-acceptor-radical (D−B-A−R•) compounds.[18c] In their study, the acceptor part was excited and an electron was transferred from D to ^{3}A*, as represented by ^{4}[D−B−^{3}A*−^{2}R•] → ^{4}[D$^{•+}$−B−A$^{•-}$−R•]. (c) Conti, F.; Corvaja, C.; Gattazzo, C.; Toffoletti, A.; Bergo, P.; Maggini, M.; Scorrano, G.; Prato, M. *Phys. Chem. Chem. Phys*. **2001**, *3*, 3526.

(19) (a) Mori, Y.; Sakaguchi, Y.; Hayashi, H. *Chem. Phys. Lett*. **1998**, *286*, 446. (b) Mori, Y.; Sakaguchi, Y.; Hayashi, H. *J. Phys. Chem. A* **2000**, *104*, 4896. (c) Mori, Y.; Hoshino, M.; Hayashi, H. *Mol. Phys*., in press.

(20) Mori, Y.; Sakaguchi, Y.; Hayashi, H. *Chem. Phys. Lett*. **1999**, *301*, 365.

(21) (a) Osuka, A.; Zhang, R.-P.; Maruyama, K.; Ohno, T.; Nozaki, K. *Bull. Chem. Soc. Jpn*. **1993**, *66*, 3773. (b) Osuka, A.; Nakajima, S.; Maruyama, K.; Mataga, N.; Asahi, T.; Yamazaki, I.; Nishimura, Y.; Ohno, T.; Nozaki, K. *J. Am. Chem. Soc*. **1993**, *115*, 4577. (c) Osuka, A.; Nakajima, S.; Okada, T.; Taniguchi, S.; Nozaki, K.; Ohno, T.; Yamazaki, I.; Nishimura, Y.; Mataga, N. *Angew. Chem., Int. Ed. Engl*. **1996**, *35*, 92. (d) Osuka, A.; Marumo, S.; Mataga, N.; Taniguchi, S.; Okada, T.; Yamazaki, I.; Nishimura, Y.; Ohno, T.; Nozaki, K. *J. Am. Chem. Soc*. **1996**, *118*, 155. (e) Shiratori, H.; Ohno, T.; Nozaki, K.; Osuka, A. *Chem. Commun*. **1999**, 2181. (f) Shiratori, H.; Ohno, T.; Nozaki, K.; Yamazaki, I.; Nishimura, Y.; Osuka, A. *J. Org. Chem*. **2000**, *65*, 8747.

(22) Wiederrecht, G. P.; Miemczyk, M. P.; Svec, W. A.; Wasielewski, M. R. *J. Am. Chem. Soc*. **1996**, *118*, 81.

(23) Fajer, J.; Borg, D. C.; Forman, A.; Dolphin, D.; Felton, R. H. *J. Am. Chem. Soc*. **1970**, *92*, 3451.

(24) (a) Murov, S. L.; Carmichael, I.; Hug, G. L. *Handbook of Photochemistry*, Second Edition; Marcel Dekker: New York and Basel, 1993; p. 42. (b) Tran-Thi, T. H.; Desforge, C.; Thiec, C.; Gaspard, S. *J. Phys. Chem*. **1989**, *93*, 1226. (c) Walters, V. A.; de Paula, J. C.; Jackson, B.; Nutaitis, C.; Hall, K.; Lind, J.; Cardozo, K.; Raible, D.; Phillips, C. M. *J. Phys. Chem*. **1995**, *99*, 1166.

(25) (a) Warman, J. M.; de Haas, M. P.; Verhoeven, J. W.; Paddon-Row: M. N. *Electron Transfer: from Isolated Molecules to Biomolecules. Part I and II*, Bixon, M., Jortner, J., Eds.; Wiley: New York; 1999; pp. 571−601. (b) Warman, J. M.; Smit, K. J.; de Haas, M. P.; Jonker, S. A.; Paddon-Row: M. N.; Oliver, A. M.; Kroon, J.; Oevering, H.; Verhoeven, J. W. *J. Phys. Chem*. **1991**, *95*, 1979.

(26) (a) Kaholek, M.; Hrdlovic, P. *J. Photochem. Photobiol. A: Chem*. **1999**, *127*, 45. (b) Blough, N. V.; Simpson, D. J. *J. Am. Chem. Soc*. **1988**, *110*, 1915. (c) Green, S. A.; Simpson, D. J.; Zhou, G.; Ho, P. S.; Blough, N. V. *J. Am. Chem. Soc*. **1990**, *112*, 7337. (d) Herbelin, S. E.; Blough, N. V. *J. Phys. Chem. B* **1998**, *102*, 8170.

(27) Häberle, T.; Hirsch, J.; Pöllinger, F.; Heitele, H.; Michel-Beyerle, M. E.; Anders, C.; Döhling, A.; Kriger, C.; Rückemann, A.; Staab, H. A. *J. Phys. Chem*. **1996**, *100*, 18 269, and references therein.

(28) In the case of either **1R•** or **2R•**, ^{3}ZP* was not quenched by R•. The lack of intramolecular triplet−doublet quenching for [^{3}ZP*−B−NI−R•] was probably due to the large distance between ^{3}ZP* and R• and the triplet excitation energy of ZP lower than the excitation energy of R•.

(29) In PenOAc, THF, or PrCN, fitting of the $\Delta A_{470}(t)$ curve observed for **1** under a zero field to a single-exponential function was not successful. Intramolecular decay process was so slow that bimolecular CR (2 ^{3}[ZP$^{•+}$−B$_1$−NI$^{•-}$] → [ZP$^{•+}$−B$_1$−NI] + [ZP−B$_1$−NI$^{•-}$]) might also take place. In the presence of magnetic fields, $|T_{+1}\rangle$, $|T_0\rangle$, and $|T_{-1}\rangle$ sublevels should exhibit different decay kinetics, which makes the analyses quite difficult. Therefore, we use the $R(B)$ value as a qualitative measure representing the MFEs.

(30) The plot of the ratio, $\Delta A_{470}(t, B)/\Delta A_{470}(t, 0\ \mathrm{T})$, vs t increased with t and then became constant, because the T−T absorption of ^{3}ZP* also contribute $\Delta A_{470}(t)$ to at early time. We use the constant part to obtain the $R(B)$ value.

(31) For derivation of k^S_{CR} and k_{ST} from the observed decay rates, see ref 18.

(32) (a) Fleischer, E. B.; Miller, C. K.; Webb, L. E. *J. Am. Chem. Soc*. **1964**, *86*, 2342. (b) Glick, M. D.; Cohen, G. H.; Hoard, J. L. *J. Am. Chem. Soc*. **1967**, *89*, 1996.

(33) (a) For example, the torsional angles between the porphyrin macrocycle and the peripheral phenyl groups are somewhat smaller in Zn(tpp)$^{•+}$ than Zn(tpp).[33b] (b) Spaulding, L. D.; Eller, P. G.; Bertrand, J. A.; Felton, R. H. *J. Am. Chem. Soc*. **1974**, *96*, 982.

(34) (a) Shephard, M. J.; Paddon-Row: M. N. *J. Phys. Chem. A*, **1999**, *103*, 3347. (b) Shephard, M. J.; Paddon-Row: M. N. *J. Phys. Chem. A* **2000**, *104*, 11 628. (c) Koeberg, M.; de Groot, M.; Verhoeven, J. W.; Lokan, N. R.; Shephard, M. J.; Paddon-Row: M. N. *J. Phys. Chem. A* **2001**, *105*, 3417.

(35) (a) $\Delta G^{S(T)}_{CS}$ value is estimated by the following equation:[35b] $\Delta G_{S(T)CS} = F(E^D_{OX} - E^A_{RED})_{PrCN} - e^2/(4\pi\epsilon_0\epsilon_r R_{DA}) + e^2/(8\pi\epsilon_0)(1/r_D + 1/r_A)(1/\epsilon_r - 1/\epsilon_{PrCN}) - E_{S(T)}$ Here, E^D_{OX} and E^A_{RED} are the oxidation potential of D and the reduction potential of A, respectively, measured in PrCN. $E_{S(T)}$ is the singlet (triplet) excitation energy. ϵ_r and ϵ_{PrCN} are the relative permittivities of the solvent used for the ET reaction and of PrCN, respectively. The ionic radii of D$^{•+}$ and A$^{•-}$ are denoted by r_D and r_A, respectively. Here, $r_D = 5.5$ and $r_A = 3.5$ (for NI) or 3.3 (for B$_2$) Å were used. R_{DA} is the center-to-center distance between D$^+$ and A$^-$. Here, $R_{DA} = 14$ (for **1**), 18 (between ZP and NI in **2**), or 12.5 (between ZP and B$_2$ in **2**) Å was used. (b) Rehm, D.; Weller, A. *Isr. J. Chem*. **1970**, *8*, 259.

(36) Khajehpour M.; Kauffman, J. F. *J. Phys. Chem. A* **2001**, *105*, 10 316.

(37) In literature on sequential multistep ET processes, compounds such as **2** are usually referred to as donor−primary acceptor−secondary acceptor (D−A$_1$−A$_2$) triad.

(38) Ohkohchi, M.; Takahashi, A.; Mataga, N.; Okada, T.; Osuka, A.; Yamada, H.: Maruyama, K. *J. Am. Chem. Soc*. **1993**, *115*, 12 137.

(39) *Electron Transfer: from Isolated Molecules to Biomolecules. Parts I and II*; Bixon, M., Jortner, J., Eds.; Wiley: New York, 1999.

(40) (a) Bixon, M.; Jortner, J. *J. Am. Chem. Soc*. **2001**, *123*, 12 556. (b) Sartor, V.; Boone, E.; Schuster, G. B. *J. Phys. Chem. B* **2001**, *105*, 11 057.

(41) Sumi, H.; Kakitani, T. *J. Phys. Chem. B* **2001**, *105*, 9603.

(42) Krasnovsky, Jr.; Bashtanov, M. E.; Drozdova, N. N.; Liddell, P. A.; Moore, A. L.; Moore, T. A.; Gust, D. *J. Photochem. Photobiol. A: Chem*. **1997**, *102*, 157.

(43) (a) Marcus, R. A. *J. Chem. Phys*. **1956**, *24*, 966. (b) Marcus, R. A. *J. Chem. Phys*. **1956**, *24*, 979.

(44) Sumida, J. P.; Liddell, P. A.; Lin, S.; Macpherson, A. N.; Seely, G. R.; Moore, A. L.; Moore, T. A.; Gust, D. *J. Phys. Chem. A* **1998**, *102*, 5512.

(45) The $(\Delta G^{S}_{CR} + \lambda)$ values for **1** were estimated to be −52, −31, +15, and +28 kJ mol^{-1} in PenOAc, THF, PrCN, and MeCN, respectively. The corresponding values for **2** were −46, −15, +35, and +49 kJ mol^{-1} in the same order of solvents. Here, $\lambda = \lambda_{vib} + \lambda_{out}$, λ_{vib} was assumed to be 30 kJ mol^{-1} (ca. 0.3 eV) in either solvent,[46] and λ_{out} was estimated by the equation for the dielectric continuum model.[47]

(46) (a) For several porphyrin−quinone dyads, λ_{vib} was reported to be 0.2−0.4 eV.[44,46b−d] (b) Gaines, G. L.; O'Neil, M. P.; Svec, W. A.; Niemczyk, M. P.; Wasielewski, M. R. *J. Am. Chem. Soc*. **1991**, *113*, 719. (c) Heitele, H.; Pöllinger, F.; Häberle, T.; Michel-Beyerle, M. E.; Staab, H. A. *J. Phys. Chem*. **1994**, *98*, 7402. (d) Tsue, H.; Imahori, H.; Kaneda, T.; Tanaka, Y.; Okada, T.; Tamaki, K.; Sakata, Y. *J. Am. Chem. Soc*. **2000**, *122*, 2279.

(47) The outer-sphere reorganization energy (λ_{out}) can be estimated by the following equation:[43] $\lambda_{out} = e^2/(8\pi\epsilon_0) \times (1/r_D + 1/r_A - 2/R_{DA}) \times (1/n^2 - 1/\epsilon_r)$, where n is the refractive index of the medium.

(48) Bencini, A.; Gattenschi, D. *EPR of Exchange Coupled Systems;* Springer-Verlag: Berlin, 1990.

(49) Lahti, P. M. *Magnetic Properties of Organic Materials*; Marcel Dekker: New York and Basel, 1999.

(50) (a) Kumai, R.; Matsushita, M. M.; Izuoka, A.; Sugawara, T. *J. Am. Chem. Soc*. **1994**, *116*, 4523. (b) Schultz, D. A.; Farmer, G. T. *J. Org. Chem*. **1998**, *63*, 6254. (c) Teki, Y.; Ismagilov, R. F.; Nelsen, S. F. *Mol. Cryst. Liq. Cryst*. **1999**, *334*, 313. (d) Domingo, V. M.; Burdons, X.; Brillas, E.; Carilla, J.; Ruis, J.; Torrelles, X.; Juliá, L. *J. Org. Chem*. **2000**, *65*, 6847. (e) Sakurai, H.; Izuoka, A.; Sugawara, T. *J. Am. Chem. Soc*. **2000**, *122*, 9723.

(51) (a) Sugimoto, T.; Yamaga, S.; Nakai, M.; Ohmori, K.; Tsujii, M.; Nakatsuji, H.; Fujita, H.; Yamauchi, J. *Chem. Lett*. **1993**, 1361. (b) Fujiwara, H.; Kobayashi, H. *Chem. Commun*. **1999**, 2417.

(52) The *J*-resonance valley in Figure 4a was rather broad. Such a width much larger than $|A_{HFC}|$ can be ascribed to the conformational heterogeneity (see Section 3.1) and the lifetime-broadening[10b,53d] due to the fast decay of the $|S\rangle$ state. In dioxane, the fast equilibration between the $|T\rangle$ state and [^{3}ZP*−B$_1$−NI] (see Section 3.4(a)) may further increase the width.

(53) (a) Sekiguchi, S.; Kobori, Y.; Akiyama, K.; Tero-Kubota, S. *J. Am. Chem. Soc*. **1998**, *120*, 1325. (b) Kobori, Y.; Sekiguchi, S.; Akiyama, K.; Tero-Kubota, S. *J. Phys. Chem. A*, **1999**, *103*, 5416. (c) Kobori, Y.; Akiyama, K.; Tero-Kubota, S. *J. Chem. Phys*. **2000**, *113*, 465. (d) Volk, M.; Häberle, T.; Feick, R.; Ogrodnik, A.; Michel-Beyerle, M. *J. Phys. Chem*. **1993**, *97*, 9831. (e) Bixon, M.; Jortner, J.; Michel-Beyerle, M. E. *Z. Phys. Chem*. **1993**, *180*, 193. (f) Okamura, M. Y.; Isaacson, R. A.; Feher, G. *Biochim. Biophys. Acta* **1979**, *546*, 394.

(54) In a region of $(\Delta G^{S}_{CR} + \lambda) \cong 0$, eq 6 is not valid. The theoretical studies predicted that the *J* value becomes zero at $\Delta G^{S}_{CR} + \lambda = 0$ and changes in sign from positive to negative with increase in $(\Delta G^{S}_{CR} + \lambda)$.[53c−e] Such ΔG dependence of *J* was also observed experimentally for solvent-separated radical ion-pairs generated through intermolecular photoinduced ET reactions.[12b,53a,b] For the CS states generated through intramolecular ET in the D−B−A compounds, positive *J* values were also observed in case that the CR processes fall in the inverted region.[10b]

(55) According to ref 53d, e, treatment of *J* as a weighted summation of the contributions from each of the vibronic states gives smaller $(\Delta G + \lambda)$-dependence than expected from eq 6. This may also explain the similarity in the *J* values observed in THF and PenOAc.

(56) (a) $B_{1/2} = 2\,(|A_{HFC}(1)|^2 + |A_{HFC}(2)|^2)/(|A_{HFC}(1)| + |A_{HFC}(2)|)$; $|A_{HFC}(i)| = [\Sigma_j\, I_j(I_j + 1)\, a_j^2]^{1/2}$ (i = 1, 2), where I_j and a_j are the nuclear spin quantum number and the isotropic HFC constant, respectively, of the j-th nucleus. (b) Schulten, K.; Wolynes, P. G. J. *Chem. Phys*. **1978**, *68*, 3292.

(57) (a) The *J* value for each pair of radicals in [ZP$^{\bullet+}$−B−NI$^{\bullet-}$−R•] may be different from that for each two-spin system, [NI$^{\bullet-}$−R•], [ZP$^{\bullet+}$−B−NI$^{\bullet-}$], or [ZP$^{\bullet+}$−B−NI−R•].[57b−d] (b) Turek and Catala reported that the *J* value of a radical pair can be changed by the presence of another radical. (c) Catala, L.; Turek, P. *J. Chim. Phys*. **1999**, *96*, 1551. (d) Catala, L.; Turek, P.; Le Moigne, J.; De Cian, A.; Kyritsakas, N. *Tetrahedron Lett*. **2000**, *41*, 1015.

(58) *Organic Solvents*, 4th ed.; Riddick, J. A., Bunger, W. B., Sakano, T. K., Eds.; Wiley: New York, 1986.

(59) (a) Levin, P. P.; Batova, E. E.; Shafirovich, V. Ya. *Chem. Phys*. **1990**, *142*, 279. (b) Shafirovich, V. Ya.; Batova, E. E.; Levin, P. P. *J. Chem. Soc., Faraday Trans*. **1992**, *88*, 935. (c) Shafirovich, V. Ya.; Levin, P. P. *Russ. Chem. Bull. Int. Ed*. **2001**, *50*, 599.

(60) Saito, T.; Hirata, Y.; Sato, H.; Yoshida, T.; Mataga, N. *Bull. Chem. Soc. Jpn*. **1988**, *61*, 1925.

(61) (a) Step, E. N.; Buchachenko, A. L.; Turro, N. J. *J. Am. Chem. Soc*. **1994**, *116*, 5462. (b) Buchachenko, A. L.; Berdinsky, V. L. *Russ. Chem. Bull*. **1995**, *44*, 1578; Translated from *Izv. Akad. Nauk. Ser. Khim*. **1995**, 1646. (c) Buchachenko, A. L.; Berdinsky, V. L. *J. Phys. Chem*. **1996**, *100*, 18 292. (d) Buchachenko, A. L.; Berdinsky, V. L.; Turro, N. J. *Kinetics and Catalysis* **1998**, *39*, 301; Translated from *Kinetika i Kataliz* **1998**, *39*, 325. (e) Buchachenko, A. L.; Berdinsky, V. L. *Chem. Phys. Lett*. **1998**, *298*, 279. (f) Buchachenko, A. L.; Berdinsky, V. L. *Chem. Rev*. **2002**, *102*, 603.

(62) Schulten, K. *J. Chem. Phys*. **1984**, *80*, 3668.

(63) Although the $|A_{HFC}|$ value of R• is larger than that of ZP$^{\bullet+}$ or NI$^{\bullet-}$, the energy gap between the $|D\rangle$ and $|Q\rangle$ states (which is represented by the equation in ref 61) is much larger than these $|A_{HFC}|$ values because of $|J(NI^{\bullet-}, R\bullet)| \gg |J(ZP^{\bullet+}, NI^{\bullet-})|$.

(64) (a) Atkins, P. W.; Evans, G. T. *Mol. Phys*. **1975**, *29*, 921. (b) Iwasaki, Y.; Maeda, K.; Murai, H. *J. Phys. Chem. A* **2001**, *105*, 2961.

(65) (a) Hayashi, H.; Itoh, K.; Nagakura, S. *Bull. Chem. Soc. Jpn*. **1966**, *39*, 199. (b) Itoh, K.; Hayashi, H.; Nagakura, S. *Mol. Phys*. **1969**, *17*, 561. (c) Kaptein, R. *J. Am. Chem. Soc*. **1972**, *94*, 6251.

(66) The $|S\rangle \leftrightarrow |T_0\rangle$ conversion is a coherent process and in general cannot be described adequately by a rate. In the present paper, however, we did not use stochastic treatment but analyzed the decay curves using exponential functions and describe the probability of the change in spin multiplicity as a first-order rate constant, k_{ST}.

(67) Hamilton, D. G.; Prodi, L.; Feeder, N.; Sanders, J. K. M. *J. Chem. Soc., Perkin Trans. 1* **1999**, 1057.

(68) (a) Hosoi, H.; Mori, Y.; Masuda, Y. *Chem. Lett*. **1998**, 177. (b) Hosoi, H.; Masuda, Y. *J. Mol. Liq*. **2001**, *90*, 279.

(69) *WIN−SimFonia*, EPR Simulation Software, Brucker.

(70) (a) Hay, P. J.; Wadt, W. R. *J. Chem. Phys*. **1985**, *82*, 270. (b) Wadt, W. R.; Hay, P. J. *J. Chem. Phys*. **1985**, *82*, 284. (c) Hay, P. J.; Wadt, W. R. *J. Chem. Phys*. **1985**, *82*, 299.

(71) (a) Becke, A. D. *J. Chem. Phys*. **1993**, *98*, 5648. (b) Lee, C.; Yang, W.; Parr, R. G. *Phys. Rev. B* **1988**, *37*, 785.

(72) Frisch, M. J.; Trucks, G. W.; Schlegel, H. B.; Scuseria, G. E.; Robb, M. A.; Cheeseman, J. R.; Zakrzewski, V. G.; Montgomery, J. A. Jr.; Stratmann, R. E.; Burant, J. C.; Dapprich, S.; Millam, J. M.; Daniels, A. D.; Kudin, K. N.; Strain, M. C.; Farkas, O.; Tomasi, J.; Barone, V.; Cossi, M.; Cammi, R.; Mennucci, B.; Pomelli, C.; Adamo, C.; Clifford, S.; Ochterski, J.; Petersson, G. A.; Ayala, P. Y.; Cui, Q.; Morokuma, K.; Malick, D. K.;. Rabuck, A. D.; Raghavachari, K.; Foresman, J. B.; Cioslowski, J.; Ortiz, J. V.; Baboul, A. G.; Stefanov, B. B.; Liu, G.; Liashenko, A.; Piskorz, P.; Komaromi, I.; Gomperts, R.; Martin, R. L.; Fox, D. J.; Keith, T.; Al-Laham, M. A.; Peng, C. Y.; Nanayakkara, A.; Gonzalez, C.; Challacombe, M.; Gill, P. M. W.; Johnson, B.; Chen, W.; Wong, M. W.; Andres, J. L.; Gonzalez, C.; Head-Gordon, M.; Replogle, E. S.; Pople, J. A. *Gaussian 98*, Revision A.7, Gaussian, Inc., Pittsburgh, PA, 1998.

(73) Kobori, K.; Takeda, K.; Tsuji, K.; Kawai, A.; Obi, K. *J. Phys. Chem. A* **1998**, *102*, 5160.

(74) *Handbook of Chemistry and Physics*, 77th ed.; Lide, D. R., Ed.; CRC Press: Boca Raton, FL, 1996; pp 6−151.

(75) Huber, M.; Galili, T.; Möbius, K.; Levanon, H. *Isr. J. Chem*. **1989**, *29*, 65.